MASTERARBEIT | MASTER'S THESIS

Titel | Title

Effect of Holocene environmental change on the size structure of mollusk indicator species of the northern Adriatic Sea

verfasst von | submitted by

Lukas Schweigl BSc BSc

angestrebter akademischer Grad | in partial fulfilment of the requirements for the degree of

Master of Science (MSc)

Wien | Vienna, 2024

Studienkennzahl lt. Studienblatt | Degree programme code as it appears on the student record sheet:	UA 066 815
Studienrichtung lt. Studienblatt | Degree programme as it appears on the student record sheet:	Masterstudium Erdwissenschaften
Betreut von | Supervisor:	Univ.-Prof. Mag. Dr. Martin Zuschin
Mitbetreut von | Co-Supervisor:	Mag. Dr. Rafal Nawrot

Abstract

Pollution, bottom trawling, eutrophication, and frequent hypoxic events have profoundly impacted benthic soft-bottom communities in the northern Adriatic Sea (NAS). While changes in species abundance and overall community structure have been well documented, the effects of anthropogenic disturbances on body size – an important functional trait – are less understood. Previous research has shown that the opportunistic bivalve *Varicorbula gibba* not only increased in relative abundance but also in size in response to the anthropogenic stressors of the late 20th century. This study compares the size changes of *V. gibba* to those of the gastropod *Turritellinella tricarinata*, a previously common species that declined in abundance during the same period, to test for differential size responses between species with varying environmental tolerances. Additionally, long-term trends in body size during the Holocene were analyzed to establish a baseline against which the recent size changes can be evaluated.

The study utilized material from sediment cores collected at four stations across the NAS. In the eastern part of the NAS, new material from Koper Bay in the southern Gulf of Trieste provided a record extending back over 7,000 years. At this station, community composition shifted from the transgressive phase to the highstand phase as the sediment became coarser. Both *V. gibba* and *T. tricarinata* remained abundant throughout the recorded period, but their sizes changed. *V. gibba* increased in size during the highstand phase, possibly due to recurring hypoxic events following the onset of modern circulation patterns at the time of maximum flooding. Conversely, *T. tricarinata* decreased in size, potentially due to increased drilling predation or decreased nutrient input. Size patterns at this station may also have been influenced by high-energy events that caused size sorting of death assemblages.

The other stations, located in the Po and Isonzo prodeltas in the western and eastern NAS, respectively, provided records extending back 150 to 500 years. These stations experienced significant eutrophication and frequent hypoxic events during the late 20th century, which led to increases in both the abundance and size of *V. gibba*. Predatory and competitive release, along with increased nutrient input, likely caused this pattern. In contrast, *T. tricarinata* exhibited a decline in abundance and showed variable size responses to late 20th-century disturbances. In the Po prodelta, population declines of *T. tricarinata* likely led to recruitment failure, resulting in populations dominated by large adults. In the Isonzo prodelta, local extirpations followed by unsuccessful reestablishment attempts may have resulted in the accumulation of shells of small juveniles. The size increase of *V. gibba* during the late 20th century appears unique within the Holocene, while the recent size variability in *T. tricarinata* falls within the natural range of variability for this species during the Holocene. This study demonstrates that species with different ecological characteristics exhibit markedly different size responses to anthropogenic stressors.

Zusammenfassung

Meeresverschmutzung, Schleppnetzfischerei, Eutrophierung und häufige hypoxische Ereignisse haben die benthischen Weichboden-Gemeinschaften der Nordadria stark beeinflusst. Während Veränderungen in der Artenhäufigkeit und der Gesamtstruktur der Artengemeinschaft gut dokumentiert sind, sind die Auswirkungen anthropogener Störungen auf die Körpergröße - ein wichtiges funktionelles Merkmal - weniger gut verstanden. Frühere Studien haben gezeigt, dass die opportunistische Muschel *Varicorbula gibba* als Reaktion auf die anthropogenen Störungen des späten 20. Jahrhunderts nicht nur in ihrer relativen Häufigkeit, sondern auch in ihrer Größe zugenommen hat. Diese Studie vergleicht die Größenveränderungen von *V. gibba* mit denen der Schnecke *Turritellinella tricarinata*, einer früher häufigen Art, die im selben Zeitraum in ihrer Häufigkeit abnahm, um unterschiedliche Größenreaktionen zwischen Arten mit unterschiedlichen ökologischen Toleranzen zu testen. Darüber hinaus wurden langfristige Trends in der Körpergröße während des Holozäns analysiert, um eine Baseline zu schaffen, gegen die jüngste Größenveränderungen bewertet werden können.

Diese Studie verwendete Material aus Sedimentkernen, die an vier Stationen in der Nordadria gesammelt wurden. Ein Sedimentkern aus der Koper-Bucht im südlichen Golf von Triest in der östlichen Nordadria lieferte neues Material, welches teilweise mehr als 7.000 Jahre alt ist. An dieser Station änderte sich die Zusammensetzung der Artengemeinschaft von der Transgressionsphase zur Hochstandsphase, als das Sediment grobkörniger wurde. Sowohl *V. gibba* als auch *T. tricarinata* blieben während des gesamten erhaltenen Zeitraums häufig, aber ihre Größen änderten sich. *V. gibba* zeigte während der Hochstandsphase eine Größenzunahme, möglicherweise aufgrund wiederkehrender hypoxischer Ereignisse nach dem Einsetzen moderner Zirkulationsmuster zur Zeit der maximalen Transgression. Im Gegensatz dazu nahm die Größe von *T. tricarinata* ab, möglicherweise aufgrund erhöhter Prädation durch schalenbohrende Mollusken oder verringerter Nährstoffzufuhr. Die Größenmuster an dieser Station könnten auch durch hochenergetische Ereignisse beeinflusst worden sein, die zu einer Größen-Sortierung führten.

Material aus den anderen Stationen, die sich in den Prodeltas des Po und Isonzo in der westlichen bzw. östlichen Nordadria befinden, ist bis zu 150 bzw. 500 Jahre alt. Diese Stationen waren während des späten 20. Jahrhunderts stark von Eutrophierung und häufigen hypoxischen Ereignissen betroffen, was zu einer Zunahme sowohl der Häufigkeit als auch der Größe von *V. gibba* führte. Die Abnahme der Populationen von Prädatoren und Konkurrenten sowie eine erhöhte Nährstoffzufuhr trugen wahrscheinlich zu diesen Trends bei. Im Gegensatz dazu zeigte *T. tricarinata* einen Rückgang der Häufigkeit und variierte in ihrer Größenreaktion auf die Störungen des späten 20. Jahrhunderts. Im Po-Prodelta führte der Rückgang der Populationen von *T. tricarinata* wahrscheinlich zu einem

Reproduktionsversagen, was zu Populationen führte, die von großen, ausgewachsenen Tieren dominiert wurden. Im Isonzo-Prodelta könnten lokales Aussterben, gefolgt von erfolglosen Wiederansiedlungsversuchen, zur Ansammlung der Schalen kleiner Jungtiere geführt haben. Die Größenzunahme von *V. gibba* im späten 20. Jahrhundert erscheint einzigartig im Holozän, während die jüngste Größenvariabilität bei *T. tricarinata* innerhalb des natürlichen Variabilitätsbereichs dieser Art während des Holozäns liegt. Diese Studie zeigt, dass Arten mit unterschiedlichen ökologischen Merkmalen in Bezug auf ihre Größe sehr verschieden auf anthropogene Stressoren reagieren.

Contents

Introduction

Humans have altered marine ecosystems for centuries to millennia (Jackson, 2001; Lotze et al., 2011; Rick and Erlandson, 2008). Ecological monitoring, however, often started only a few decades ago. Paleobiological data from the young fossil record of the late Quaternary can be used to discern ecological changes driven by anthropogenic stressors prior to the onset of monitoring and establish a natural range of variability of an ecosystem against which recent changes can be assessed (Dietl et al., 2015; Kidwell, 2015; Kosnik and Kowalewski, 2016).

The death assemblages of the young fossil record are affected by time averaging, the accumulation of skeletal remains representing multiple generations of organisms. Consequently, they are not affected by short-term variability and well suited to study long-term trends. Sediment cores sample death assemblages far back in time and are therefore perfect for this purpose (Kidwell and Tomasovych, 2013; Kosnik and Kowalewski, 2016).

Mollusks constitute a taxon well suited for studies of long-term trends from death assemblages. They are often the most diverse taxon in death assemblages because of the high durability of their shells. Furthermore, they are among the most abundant and diverse taxa of the marine benthos and fulfill a variety of ecological roles (Kidwell, 2009). It has also been demonstrated that they can be used as surrogate for other taxa to faithfully record community-level ecological patterns, both in living and death assemblages (Tyler and Kowalewski, 2017).

The northern Adriatic Sea (NAS), a shallow epicontinental sea situated between the Balkan and Italian peninsulas, has been affected by human activity for millennia. Anthropogenic impacts intensified during the last two centuries because of industrialization and the onset of globalization (Lotze et al., 2011). This has led to modern mollusk assemblages differing significantly from those of the pre-impact Holocene and late Pleistocene interglacial (Kowalewski et al., 2015). The baseline communities of the pre-impact Holocene were spatially diverse and recent developments led to their homogenization (Gallmetzer et al., 2019). Furthermore, modern assemblages are characterized by higher degree of infaunalization and higher relative abundance of filter- and deposit feeders (Haselmair et al., 2021).

Two main drivers of these trends of homogenization and infaunalization could be discerned: 1) an increase in fishing practices such as bottom trawling and hydraulic dredging which led to a decline in epibenthic species (Gallmetzer et al., 2019; Haselmair et al., 2021; Mautner et al., 2018) and 2) a trend of eutrophication related to the strong increase in use of fertilizers, especially in the second half of the 20th century, in the areas surrounding the NAS. Apart from its direct effects, eutrophication also led to an increase in hypoxia frequency resulting from the combined effect of algal blooms and seasonal water stratification. These hypoxic events, lasting 5 to 25 days, regularly led to mass mortalities in the NAS during the

second half of the 20th century (Justić, 1991).

Eutrophication and increased hypoxia frequency had a significant effect on soft bottom communities of the NAS. Studies of death assemblages from sediment cores (Albano et al., 2018; Gallmetzer et al., 2017; Tomašových et al., 2018, 2017), as well as ecological monitoring studies (Chiantore et al., 2001; Crema et al., 1991) found that the bivalve *Varicorbula gibba*[1] became the dominant mollusk species of these communities during the late 20th century, while previously abundant mollusks such as the gastropod *Turritellinella tricarinata*[2] declined. *V. gibba* is a sedentary, infaunal suspension feeder (Hrs-Brenko, 2006; Yonge, 1946), which can cope with high levels of pollution and eutrophication (Moraitis et al., 2018), and very low oxygen levels (Holmes and Miller, 2006; Riedel et al., 2012). Its high tolerance of environmental disturbances makes *V. gibba* an opportunistic species that can become dominant in benthic communities during recolonization after disturbance events (Nerlović et al., 2011). During the early 21st century, which showed trends of oligotrophication and less frequent hypoxic events due to environmental regulations and decreased river runoff (Giani et al., 2012; Kralj et al., 2019), *V. gibba* decreased in relative abundance (Tomašových et al., 2018).

Apart from its increase in relative abundance in the NAS during the 20th century, *V. gibba* also increased in size. Living and death assemblages from the 20th and 21st century have size distributions with higher proportions of larger size classes compared to death assemblages from the preceding centuries and millennia (Fuksi et al., 2018; Tomašových et al., 2020). Size of *V. gibba* correlates positively with geochemical indicators of eutrophication (Fuksi et al., 2018) and hypoxia frequency (Tomašových et al., 2020). Growth rates of many bivalves increase in response to eutrophication as increased nutrient supply leads to higher primary production and consequently food availability (Carmichael et al., 2012). Increased hypoxia frequency could, however, also be the main driver of the size increase of *V. gibba*, as low oxygen levels can exclude potential predators (Altieri and Diaz, 2019; Calderaro et al., 2023) and competitors (Tunnicliffe, 1981), ensuring a higher survival rate of young individuals of hypoxia-tolerant species.

V. gibba is one of the few species for which size changes in response to recent environmental change in the NAS have been studied. Thus, there remains an important knowledge gap to fill as size structure is one of the functional traits of benthic communities that can indicate the quality status of an ecosystem (Basset et al., 2008; Queirós et al., 2006; Rice et al., 2012). Differential responses in body size of species with different environmental tolerances should be tested.

Similar to *V. gibba*, *T. tricarinata* is a semi-infaunal suspension feeder preferring soft bottoms (Allmon, 1988) but it does not cope well with declining oxygen levels (Marsden et al., 2012). This led to a decrease in its relative abundance in the NAS

[1] In the literature this species is often referred to by its now invalid synonym *Corbula gibba*.
[2] In the literature this species is often referred to by its now invalid synonym *Turritella communis*.

during the second half of the 20th century (see above). Preliminary results from the area off the Po delta have indicated an increase in size, despite declines in abundance (Scheidl et al., 2021). The growth rate and consequently size of *T. tricarinata* might increase in response to eutrophication as is the case for other species of mollusks (Carmichael et al., 2012). Some mollusk species can also increase in average size despite population declines in response to eutrophication and increased hypoxia frequency because of lower recruitment of juveniles (Craig, 1994). However, hypoxic conditions may also have an opposite effect on the size structure of mollusks as their growth rates decrease (Altieri and Diaz, 2019; Altieri and Witman, 2006) and larger individuals are more severely affected (Altieri and Witman, 2006; Clark et al., 2013). Thus, it remains unclear how *T. tricarinata* responded to eutrophication and frequent hypoxia in the NAS during the 20th century and this study aims to clarify this issue.

In this study, I reconstructed how the population size structure of *T. tricarinata* responded to recent environmental change in the NAS and compared this response to that of *V. gibba* based on material from sediment cores from multiple sites across the NAS. To provide a baseline against which recent changes in size structure can be assessed, I also studied long-term size trends during the Holocene of both *T. tricarinata* and *V. gibba* based on material from an undescribed sediment core from the southern Gulf of Trieste in the NAS. These data will show whether recent responses in size structure are unprecedented during the Holocene.

Study area

The NAS has an average depth of 35 m and never exceeds 100 m. It has a cyclonic (counterclockwise) flow pattern with a low-salinity flow driven by freshwater input along the western coast and a high-salinity flow arriving from the southern parts of the Adriatic Sea along its eastern coast. This creates a pronounced salinity gradient from west to east in the NAS. Apart from thermohaline factors, water circulation of the NAS is also influenced by northeasterly Bora and southeasterly Sirocco winds (Giani et al., 2012; McKinney, 2007).

The western NAS is strongly influenced by the Po river which is the largest source of freshwater and sediment input in the whole Adriatic Sea (McKinney, 2007). Sedimentation rates in the Po prodelta are among the highest in the Adriatic Sea but part of the sedimentary input is transported southward by the cyclonic flow contributing to the mud belt along the western Adriatic Sea (Frignani et al., 2005). Nutrient input by the Po river results in eutrophic conditions in the western NAS, whereas the eastern part is mostly oligotrophic (Zavatarelli et al., 1998).

The Gulf of Trieste, located in the NE part of the study area, is a semi-enclosed basin with depths that rarely exceed 30 m (Trobec et al., 2018). Conditions in the gulf are mesotrophic due to riverine input (Zavatarelli et al., 1998). The most

important source of freshwater, nutrient, and sediment input is the Isonzo (Soča) river in the north of the gulf. Sedimentation rates in its prodelta are among the highest in the Adriatic Sea (Frignani et al., 2005). The delta lies at the entrance of the Bay of Panzano. Further bays lie in the south of the gulf including Koper Bay, a submerged valley of the Rižana river. The sediment in bays mostly comprises silt but grain size increases gradually towards the center of the gulf which is dominated by sand (Ogorelec et al., 1991).

Material and Methods

Sampling sites

The material used in this study comes from 1.50- to 1.55-m-long sediment cores from four stations within the NAS (figure 1). All cores were collected using an UWITEC® piston corer with hammer action and interchangeable core tube units (Gallmetzer et al., 2016). During a sampling campaign in 2013 cores were collected at stations Po 3 and Po 4 located in the Po prodelta and station Panzano located in the Isonzo prodelta (see table 1 for an overview of the studied stations). During a sampling campaign in 2021 cores were collected at station Koper 4 located at the transition zone from Koper Bay to the open part of the Gulf of Trieste.

Figure 1. Map of the northern Adriatic Sea (NAS) with locations of the studied stations (modified from Gallmetzer et al. (2019)).

At each station one to two 16-cm-diameter cores were taken to study changes in death assemblages. Additionally, 9-cm-diameter cores were collected at each station for ^{210}Pb dating of sediment and geochemical analyses.

Changes in faunal composition were studied for stations Po 3 and Po 4 (Albano et al., 2018; Tomašových et al., 2018)[3], as well as Panzano (Gallmetzer et al., 2017; Tomašových et al., 2017). Equally, size changes of *V. gibba* were studied for both Po stations (Albano et al., 2018; Tomašových et al., 2020), as well as Panzano (Fuksi et al., 2018; Tomašových et al., 2020). These studies also analyzed changes in concentrations of metals, nutrients, and organic pollutants as potential drivers of shifts in faunal composition and size distributions. A chronologic

[3] In Albano et al. (2018) station Po 3 is referred to as Po 2 and station Po 4 is referred to as Po 1.

framework for the cores was established based on ^{14}C-calibrated amino acid racemization dating of bivalve shells (Tomašových et al., 2018, 2017). Together with ^{210}Pb profiles along the cores these shell ages demonstrated very high sedimentation rates of over 2 cm/year for the Po stations (Albano et al., 2018; Tomašových et al., 2018) and of 0.2 to 0.48 cm/year for Panzano (Tomašových et al., 2017). Consequently, cores from these stations provide high-resolution records, which are appropriate to study size changes in response to anthropogenic impacts during the last century.

At station Koper 4 the sedimentary record is much more condensed as it lies at the transition zone to the central part of the Gulf of Trieste, which typically has a Holocene sedimentary cover of only a few meters (Trobec et al., 2018). Therefore, the core from Koper 4 has lower temporal resolution than the cores from the Po and Isonzo prodeltas but reaches further back in time and is thus well suited for studying long-term trends in size structure during the Holocene. To identify potential drivers of size shifts in *V. gibba* and *T. tricarinata* at this station, changes in faunal composition and geochemical parameters were also analyzed, as they have not been previously studied. A chronologic framework is provided by ^{14}C-dating of mollusk shells.

Table 1. Overview of stations and cores used in this study.

Area	Station (cores used for faunal & size analysis)	Coordinates	Water depth	Core chronology (lower age limit)	References
North-western Adriatic Sea (Po prodelta)	Station Po 3 (cores M13 and M14)	44° 50’ 32” N 12° 32’ 20” E	23 m	~ 150 years BP	(Albano et al., 2018; Tomašových et al., 2018)
	Station Po 4 (cores M20, M21 and S12)	44° 43’ 50” N 12° 26’ 25” E	21 m	~ 150 years BP	(Albano et al., 2018; Tomašových et al., 2018)
Northern Gulf of Trieste (Isonzo prodelta)	Station Panzano (cores M28 and M29)	45° 44’ 07” N 13° 37’ 20” E	12 m	~ 500 years BP	(Gallmetzer et al., 2017; Tomašových et al., 2017)
Southern Gulf of Trieste	Station Koper 4 (core KOP4-21-10)	45° 35’ 53” N 13° 37’ 20” E	25 m	~ 7200 years BP	This study

Sample preparation

Core KOP4-21-10 was sliced on board into 2.5-cm-increments in its upper 20 cm and into 5-cm-increments below. The 16-cm-diameter cores from stations Po 3, Po 4, and Panzano were also sliced on board into 2-cm-increments in their upper 20 cm and into 5-cm-increments below (Albano et al., 2018; Gallmetzer et al., 2017). For each increment from KOP4-21-10 subsamples (29-78 g) were taken on board and used for grain size analysis. The remaining part of each increment was sieved through a 1-mm mesh size and mollusk material used for faunal and size analysis was picked from the dried > 1-mm sieve fraction under a stereomicroscope. The same procedure was used for cores from the other stations (Albano et al., 2018; Gallmetzer et al., 2017). Because of the large amount of material present in some samples from KOP4-21-10, they were split and only one of the splits was picked. The sieved material of increments from the core depths of 20 to 35 cm and 55 to 80 cm was halved. The sieved material of increments from 35 to 50 cm depth was quartered. The >1-mm sieve fraction comprises mostly biogenic material (figure 2).

Figure 2. Left: Radiographic image of core KOP4-21-9. The lighter the grey shading, the higher the sediment density. Right: >1-mm sieve fraction of two increments (0-2.5 and 65-70 cm) from core KOP4-21-10. Note the prevalence of shells and biogenic debris.

The 9-cm-diameter core from Koper 4 (KOP4-21-9) was sealed after retrieval and sent to the Institute of Marine Sciences (ISMAR) in Venice. At ISMAR radiographic images were taken to determine density along the core (figure 2). Then the core was halved. One half was left intact for future research while the other was sliced into 2.5-cm-increments and used for ^{210}Pb dating and geochemical analyses. Unlike for Koper 4, multiple 9-cm-diameter cores were taken at Po 3, Po 4, and Panzano, of which one was used for ^{210}Pb dating and grain size analysis and another one for geochemical analyses (Albano et al., 2018; Gallmetzer et al., 2017; Tomašových et al., 2018, 2017).

Granulometry

The subsamples from KOP4-21-10 taken on board were screened through a set of four sieves (2 mm, 1 mm, 0.125 mm, 0.063 mm), dried and weighted to estimate the proportion of the gravel (> 2mm) and sand (0.063-2 mm). The proportion of pelite (< 0.063 mm) is the difference between the dried weight of the entire

subsamples and the combined weight of the gravel and sand fractions.

The proportions of gravel and sand were determined the same way for 9-cm-diameter cores from Po 3, Po 4, and Panzano. The finer fraction was analyzed with a SediGraph III 5210 Particle Size Analyzer to determine the proportions of silt (0.002-0.063 mm) and clay (< 0.002 mm) (Albano et al., 2018; Gallmetzer et al., 2017), which can be combined into the proportion of pelite.

^{210}Pb dating

To determine sedimentation rate, activities of ^{210}Pb and ^{226}Ra were analyzed for 2.5-cm-increments from the upper 42.5 cm of core KOP4-21-9 at Eawag Department Surface Waters in Switzerland. Sedimentation rate was calculated based on the slope of the decay in excess ^{210}Pb according to the Constant Flux-Constant Sedimentation model (CFCS) (Sanchez-Cabeza and Ruiz-Fernández, 2012), avoiding the surface mixed layer (SML), within which excess ^{210}Pb levels remain approximately constant.

For cores from Po 3, Po 4, and Panzano activities of ^{210}Pb and ^{226}Ra were analyzed for 2-cm-increments from the upper 20 cm and for 5-cm-increments from 20 to 40 cm by gamma spectrometry using a High Purity Germanium detector system at the Low-Level Counting Labor Arsenal at the University of Natural Resources and Life Science in Vienna. Sedimentation rates were calculated using the same approach as for Koper 4 (Albano et al., 2018; Tomašových et al., 2017).

Shell dating

To provide a chronologic framework for trends in faunal composition and size structure at Koper 4, bivalve shells from selected increments of KOP4-21-10 were age-dated by ^{14}C measurements. Ten valves of *V. gibba* were randomly selected from each of the following increments: 25-30 cm, 65-70 cm, 105-110 cm, and 145-150 cm. Only right valves of *V. gibba* were selected to avoid double-dating of the same individual. Additionally, valves of *Ostrea edulis* were selected from the following increments: 65-70 cm (1 valve), 70-75 cm (4 valves), 100-105 cm (3 valves), 105-110 cm (2 valves), and 145-150 cm (1 valve).

To avoid contamination, shells were cleaned with hydrochloric acid in an ultrasonic bath prior to ^{14}C measurements. Measurements were performed by accelerator mass spectrometry (AMS) using the Mini Carbon Dating System (MICADAS) (Synal et al., 2007) at the Arizona Climate and Ecosystems Isotope Laboratory of Northern Arizona University (see Bright et al. (2024) for further details). The ^{14}C dates obtained from these analyses were calibrated based on the calibration curve Marine20 that provides a non-polar global-average marine record of radiocarbon from 0-55000 calibrated yrs BP and serves as a baseline for regional oceanic variation (Heaton et al., 2020). Regional marine reservoir correction ΔR = -152 (± 39) for the NAS was obtained from http://calib.org/marine/ and based on ^{14}C dating in earlier studies (Peharda et al., 2019; Siani et al., 2000). Calculation of calibrated ages was performed using the rcarbon package (version 1.5.1) in R (Crema and

Bevan, 2021).

The chronologic framework for Po 3, Po 4, and Panzano was based on ^{14}C-calibrated amino acid racemization (AAR) dating of shells of *V. gibba*. 252 shells were dated from 14 increments of core M13 at station Po 3, 243 shells from 14 increments of core M21 at station Po 4, and 311 shells from 12 increments of core M28 at station Panzano. Age distributions of undated increments were calculated based on those of directly dated increments above and below (Tomašových et al., 2018, 2017).

Geochemistry

Geochemical analysis was carried out at ISMAR in Venice. Radiographic images were taken of the cores to check for down-core sediment density trends to identify the most convenient intervals for sample extraction and analysis. From Po 3 the following intervals were selected: 0-2 cm, 4-6 cm, 8-10 cm, 14-16 cm, 25-30 cm, 35-40 cm, 50-55 cm, 65-70 cm, 80-85 cm, 100-105 cm, and 115-120 cm. From Po 4 the following intervals were selected: 0-2 cm, 4-6 cm, 8-10 cm, 18-20 cm, 25-30 cm, 35-40 cm, 45-50 cm, 70-75 cm, 80-85 cm, 85-90 cm, 95-100 cm, 115-120 cm, and 135-140 cm. From Panzano the following intervals were selected: 0-2 cm, 4-6 cm, 8-10 cm, 20-25 cm, 40-45 cm, 55-60 cm, 75-80 cm, 110-115 cm, 125-130 cm, and 145-150 cm. For the core from Koper 4 all 2.5-cm-increments from 0 to 142.5 cm depth were analyzed.

For every selected increment the concentrations of heavy metals (As, Cd, Cr, Cu, Ni, Pb, Zn) and nutrients (total organic carbon – TOC, total nitrogen – TN) were measured. A detailed protocol for measurement of these geochemical parameters can be found in Vidović et al. (2016). Concentrations of geochemical parameters for Po 3 and Po 4 were discussed by Albano et al. (2018) and Tomašových et al. (2018), and for Panzano by Gallmetzer et al. (2017)[4].

Concentrations of heavy metals from each station were compared to NOAA effects range low (ERL), the threshold level below which effects on benthic organisms rarely occur, and effects range medium (ERM), above which effects are likely to occur, to look for ecologically relevant pollution levels (Buchman, 2008; Burton, 2002).

Community analysis

The following increments were selected to analyze trends in community composition of bivalves and gastropods along core KOP4-21-10: 0-2.5 cm, 2.5-5 cm, 10-12.5 cm, 12.5-15 cm, 25-30 cm, 45-50 cm, 65-70 cm, 85-90 cm, 105-110 cm, 125-130 cm, and 145-150 cm. For each of these increments picked shells were identified to species level whenever possible and counted to obtain the

[4] In these studies, the concentration of Hg and organic pollutants (polycyclic aromatic hydrocarbons - PAH, polychlorinated biphenyls – PCB) was also analyzed. No Hg measurements are available for Koper 4 and the concentrations of organic pollutants were mostly below the detection limit of the analyses performed.

number of individuals for each species. For bivalves, only shells with preserved umbo were counted and the minimum number of individuals was calculated by adding the higher number of single valves (left or right) to the number of articulated specimens. For gastropods, all shells with preserved apex were counted. Species were assigned to feeding guilds, substrate relation, and vegetation association (table 2) based on information from the supplementary material of Haselmair et al. (2021).

For community analysis the increments 0-2.5 cm and 2.5-5 cm, as well as 10-12.5 cm and 12.5-15 cm were pooled. Thus, the entire community analysis was based on 5-cm-increments. The density of bivalves and gastropods was calculated for each increment by dividing the combined number of individuals of all species by the volume of each increment. For those increments that were split before picking, the number of individuals was multiplied by the factor by which a sample was split before calculating density. Raw species richness was calculated for each increment. Furthermore, increments were rarefied to the sample size of the smallest increment (n = 288) to calculate species richness and the effective number of species (the exponential of the Shannon entropy, exp(H)) independent of sampling effort.

Table 2. Ecological guilds to which mollusk taxa from station Koper 4 were assigned (from supplementary material of Haselmair et al. (2021)).

Feeding guilds	Substrate relation	Vegetation association
herbivore	soft bottom infauna	no association
carnivore	soft bottom epifauna	mainly seagrass
filter feeding	soft bottom semi-infauna	algae and seagrass
grazing	hard bottom infauna	algae
detritivore	hard bottom epifauna	seagrass rhizome layer
chemosymbiotic	soft & hard bottom epifauna	lucinid bivalve
scavenger	epifauna on vegetation	
	soft bottom nestler	
	epibionts & ectoparasites	

Differences in community composition between increments were visualized via non-metric multi-dimensional scaling (NMDS) with two dimensions based on Bray-Curtis distances of square-root-transformed relative abundances of species. Differences in community composition between distinct units of KOP4-21-10 were also analyzed using PERMANOVA based on the same distance matrix as used for the ordination. Singletons were removed prior to these analyses. The analyses were performed using the vegan (version 2.6-6.1) and MASS packages (version 7.3-60.2) of R (Oksanen et al., 2024; Venables and Ripley, 2002).

Size analysis

Size data for *V. gibba* from Po 3 and Po 4 are from Albano et al. (2018) and were measured using a measuring stage and a stereomicroscope (Leica MZ12). Size data from Panzano are from Fuksi et al. (2018) and were measured by a Mutitoyo digital slide caliper mounted on a binocular (Leica MZ6) lens table. Specimens of *V. gibba* from Koper 4 were photographed and measured using ImageJ software by Ivana Koubová at the Earth Science Institute of the Slovak Academy of Sciences in Bratislava. Except for Koper 4, size trends of *V. gibba* were previously analyzed for all stations (Albano et al., 2018; Fuksi et al., 2018; Tomašových et al., 2020). I will discuss them, however, as a comparison to size trends in *T. tricarinata*.

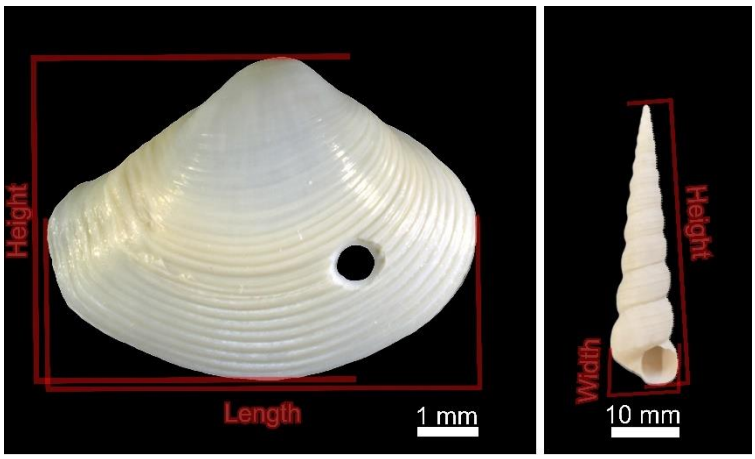

Figure 3. Measurements performed for V. gibba *(left) and* T. tricarinata *(right).*

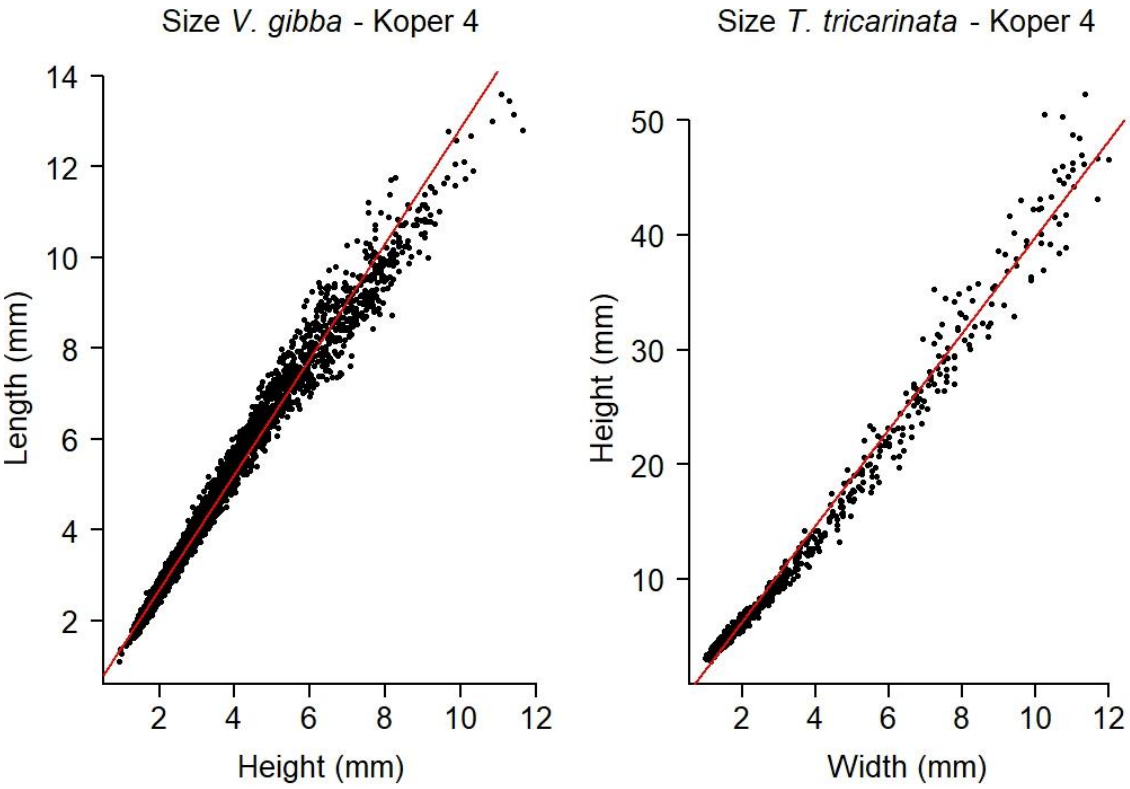

Figure 4. Relation of length and height for V. gibba (left) and width and height for T. tricarinata (right) from Koper 4. The linear regression lines are in red. The pattern is similar for data from the other stations of the NAS.

Specimens of *V. gibba* for which either length or height, or both shell dimensions could be measured were included in the size analysis (figure 3). As length and height are highly correlated (Spearman rank correlation for Koper 4, $\rho = 0.99$, $S = 137390657$, $p < 0.001$, see also figure 4), only length was used for the analysis. If only height was measured, linear regression based on the Ordinary Least Squares (OLS) method was used to calculate length from height. Furthermore, articulated specimens were used to perform linear regression to estimate the length of right valves from the length of left valves. This was necessary because the valves of *V. gibba* are very unequal in size. Thus, thanks to that approach, all measurable valves of *V. gibba* could be used for the size analysis. For *V. gibba* from Po 3, Po 4, and Panzano, linear regressions were based on data for the entire NAS from Tomašových et al. (2020). Because of the large sample size and a total of 45 articulated specimens, linear regression for Koper 4 was based only on specimens from KOP4-21-10 (table 3).

Table 3. Parameters used for linear regression to estimate length from height and right valve length from left valve length for V. gibba*. The following formula was used for linear regression: y = ax + b.*

	NAS		**Koper 4**	
	slope	**intercept**	**slope**	**intercept**
Length from Height (left valve)	1.36	- 0.12	1.41	-0.10
Length from Height (right valve)	1.20	0.27	1.22	0.24
Right valve length from left valve length	1.10	0.47	1.05	0.23

Specimens of *T. tricarinata* from Po 3 and Po 4 were measured by Paolo Albano with a caliper at the Department of Paleontology of the University of Vienna. These data were never published but discussed in an EGU poster presentation (Scheidl et al., 2021). *T. tricarinata* from Panzano and Koper 4 were photographed and measured using ImageJ software by Ivana Koubová using the same approach as for *V. gibba* from Koper 4. *T. tricarinata* from core M21 from Po 4 were also measured the same way. This allowed for a comparison between caliper and ImageJ measurements. Overall, the size trends for M21 differed only marginally between the two methods (figure 5). Thus, data based on these different measurement methods are comparable. I used caliper-measured sizes for Po 4 because only this type of data was available for the other cores from this station (M20, S12).

Specimens of *T. tricarinata* with a completely preserved aperture (fragmentation score 0, figure 6) and with a broken but still present last whorl (score 0.5) were used for size analysis. Specimens with a broken spire, where the last whorl was absent (score 1) were omitted from the analysis. In KOP4-21-10 these made up a very large portion of the specimens. Consequently, I calculated their relative proportions to check for any trends in fragmentation along the core, as this could also potentially affect the observed size structure, and compared it to the trend in

fragmentation of *V. gibba*, for which few specimens were excluded from the size analysis. I also tested how size trends would change if highly fragmented specimens, which give a minimum size estimate, were included in the analysis. For all specimens, height and width of the spire were measured (figure 3). As these variables are highly correlated (Spearman rank correlation for Koper 4, ρ = 0.99, S = 1035455, $p < 0.001$, see also figure 4), only height of the spire was used for size analysis.

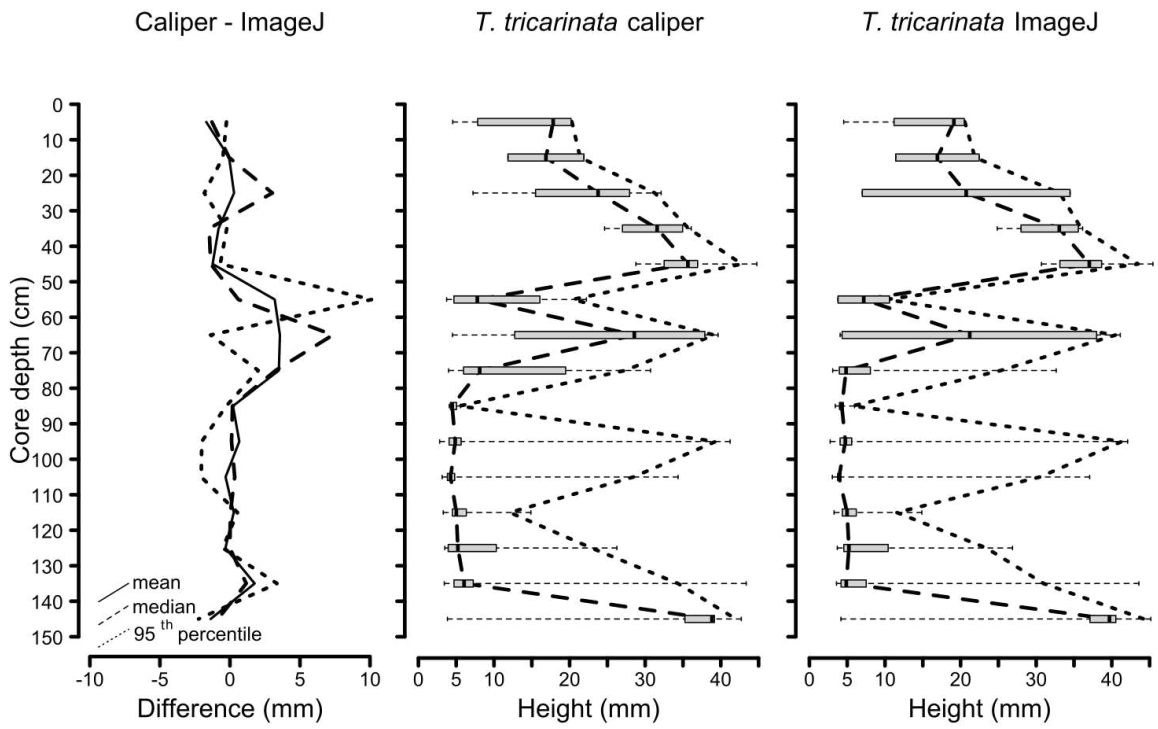

Figure 5. Comparison of size trends of T. tricarinata *from core M21 from station Po 4 based on caliper and ImageJ software measurements. Left: Difference between mean, median, and 95th percentile height of caliper and ImageJ measurements. Centre: Size trends based on caliper measurements. Right: Size trends based on ImageJ measurements.*

To study size trends, data from the 16-cm-diameter cores from Po 3, Po 4 and Panzano were pooled within each station. Size data from Po 4 also included measured specimens from a 9-cm-diameter core used for grain size analysis (S12). Cores were pooled for two reasons: 1) this was also done previously for size analysis of *V. gibba* (Albano et al., 2018; Tomašových et al., 2020) and the size trends were very similar for cores from the same station (Fuksi et al., 2018) and 2) sample sizes are very small, especially for *T. tricarinata*, for multiple increments from these three stations (sample sizes are listed in the appendix).

Because of the small sample sizes, increments from Po 3, Po 4, and Panzano were pooled into 10-cm-increments to study size trends. As both species had large sample sizes at Koper 4, trends at this station were analyzed at the level of the original 2.5- and 5-cm increments. Differences in size structure were also analyzed

at the level of stratigraphic units of the cores, which were determined based on the age distributions of shells and lithology for Po 3 and Po 4 (Tomašových et al., 2018), based on age distributions of shells for Panzano (Tomašových et al., 2017), and based on lithology for Koper 4 (see results below). To test for statistically significant differences in size distributions between the units of a given station, two-sided Wilcoxon rank-sum test (= Mann-Whitney U test), or a Kruskal-Wallis test was performed depending on the number of the units. When the result of a Kurskal-Wallis test was significant, pairwise comparisons were performed using Wilcoxon rank-sum test with Bonferroni correction. These non-parametric tests were chosen because of non-normality of size distributions.

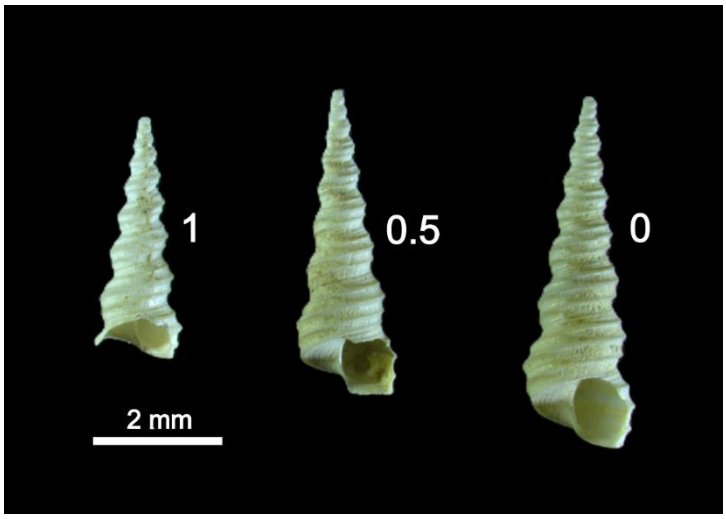

Figure 6. Specimens of T. tricarinata *from station Po 4, illustrating how shells with different degrees of fragmentation were given scores of 0, 0.5, or 1.*

Finally, differences in size distributions between core increments from all stations were visualized by NMDS based on Kolmogorov distances following an approach of De Baets et al. (2022). For this purpose, increments from Po 3, Po 4, and Panzano were pooled into 20-cm- to 65-cm-increments, which correspond to the stratigraphic units of the cores (see above). These increments can be assigned to (half-) centuries based on the age distributions of shells (Tomašových et al., 2018, 2017). 2.5-cm-increments in the upper 20 cm of Koper 4 were pooled into 5-cm-increments, otherwise the original 5-cm-increments were used for this station. 5-cm-increments were chosen because of the condensed record at Koper 4, which makes short increments more comparable than longer ones in their degree of time averaging to stratigraphic units of the other stations. All increments that had less than 20 specimens despite pooling were excluded from this analysis. Specimens from the remaining increments were assigned to size classes: 1-mm size classes from 0 to 14 mm for *V. gibba* and 5-mm size classes from 0 to 55 mm for *T. tricarinata*. The relative abundances of size classes were used to generate curves for the size distribution of each increment and then Kolmogorov distances between the curves of different increments were calculated. Then two-dimensional NMDS ordination was performed to visualize temporal and spatial differences in size structure. The vegan (version 2.6-6.1) and distrEx (version 2.9.2) packages were used for this analysis (Oksanen et al., 2024; Ruckdeschel et al., 2006). All statistical analyses in this study were performed using R version 4.4.1 (R Core Team, 2024).

Results

Trends at Koper 4

Sediment composition

Sediment from KOP4-21-10 comprises predominantly pelite throughout the core (figure 7). Unlike stations Po 3, Po 4, and Panzano, where grain size distribution is homogenous throughout the cores and the proportion of pelite is never lower than 97% (Albano et al., 2018; Gallmetzer et al., 2017), two units with distinct grain size distribution can be discerned at Koper 4, as the proportion of pelite varies from 75 to 97%. From the bottom of the core to 75 cm depth the proportion of pelite is more than 90%, except for a short interval from 105 to 115 cm depth, where values are as low as 85% and the proportion of gravel reaches up to 12%. From 75 to 60 cm depth the proportion of pelite decreases from 92 to 78%, with the proportion of gravel, which comprises mostly shells and biogenic debris (figure 3), increasing to 16%. From 60 to 2.5 cm depth the proportion of pelite fluctuates around 80%. For most of this interval the proportion of sand is higher than that of gravel. In the uppermost increment the proportion of pelite increases again to 89%. Based on this pattern of grain size distribution I divided core KOP4-21-10 into two lithologic units, with the border set at 65 cm depth.

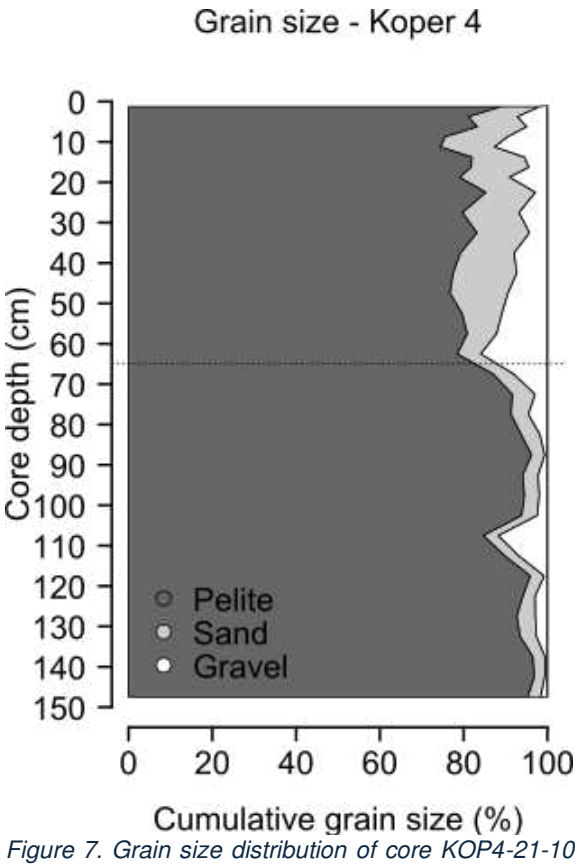

Figure 7. Grain size distribution of core KOP4-21-10 from station Koper 4.

^{210}Pb activity

In the upper 10 cm of KOP4-21-9 excess ^{210}Pb values decrease downward but at a comparatively low rate (figure 8). Therefore, the upper 10 cm are probably the surface mixed layer (SML) containing the 20th to 21st century signal.

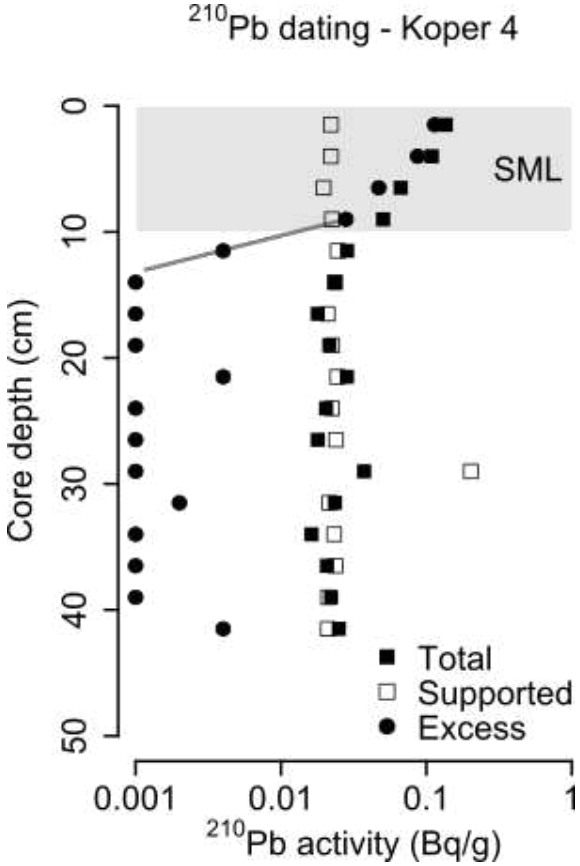

Figure 8. ^{210}Pb activity in the upper part of core KOP4-21-9 from station Koper 4.

From the increment at 7.5-10 cm to the increment at 12.5-15 cm excess values decrease at a high rate attaining a value of 0 at 12.5-15 cm. Below this interval most excess values are close to 0.001 or lower, with a few exceptions which have probably resulted from deep mixing. The slope of ^{210}Pb decay based on excess values was calculated for the interval from 7.5 to 15 cm, resulting in the following equation: $^{210}Pb_{ex} = 35.35*e^{-0.79*Depth}$. Based on the slope of decay from this interval and the ^{210}Pb disintegration constant a sedimentation rate of 0.39 mm/year was calculated for the upper part of KOP4-21-9.

Shell ages

Calibrated shell ages confirm the assumption that the record at station Koper 4 reaches far back into the early Holocene. The median age of *V. gibba* in the lowermost increment is 7160 yrs BP (see table 4 for an overview). The median ages for the increments at 105-110 cm, 65-70 cm, and 25-30 cm depth are 6752, 6068, and 2074 yrs BP, respectively. The lower three dated increments are from the lower lithologic unit of KOP4-21-10 (see above). Based on the median ages of *V. gibba,* this unit was deposited during the transgressive phase and the time of maximum flooding of the Holocene transgression (Amorosi et al., 2017; Vacchi et al., 2016). Therefore, the lower lithologic unit can be assigned to the transgressive systems tract (TST) and the maximum flooding zone (MFZ), and the upper unit to the highstand systems tract (HST).

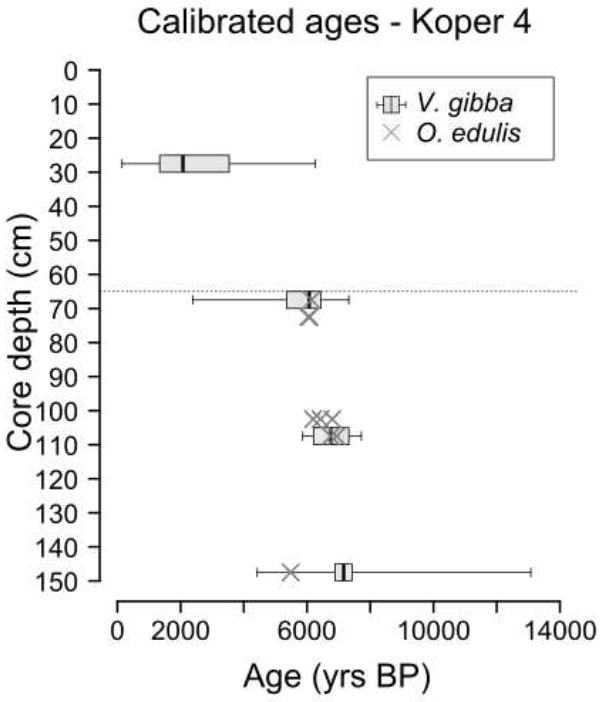

Figure 9. Calibrated ^{14}C ages of V. gibba *and* O. edulis *from core KOP4-21-10 from station Koper 4. Age distributions of* V. gibba *are shown as boxplots. Ages of* O. edulis *are shown separately for each specimen.*

Based on the median age of the lowermost increment an average sedimentation rate of 0.21 mm/year was calculated for the entire sedentary succession in KOP4-21-10. However, the sedimentation rate differed between the two stratigraphic units, reaching on average 0.73 mm/year in TST-MFZ (calculated based on the difference in median age of its lowermost and uppermost increment) and subsequently decreasing to 0.10 mm/year in the lower part of the HST (based on the difference in median age of the uppermost increment from the TST-MFZ and the dated increment at 25-30 cm depth).

The interquartile range (IQR) of the postmortem ages of *V. gibba* increases from bottom to top of the core (figure 9), ranging from 481 to 2199 yrs. In the TST-MFZ, IQRs of the adjacent dated increments overlap. The calibrated ages of *O. edulis* all

fall within the range of the ages of *V. gibba* from the same increment.

Table 4. Parameters of the age distributions of V. gibba *from core KOP4-21-10 from station Koper 4. The age distribution of each increment is based on 10 specimens.*

	Minimum	25th Perc.	Median	75th Perc.	Maximum	IQR
25-30 cm	148	1338	2074	3537	6267	2199
65-70 cm	2392	5496	6068	6408	7318	911
105-110 cm	5862	6266	6752	7198	7717	932
145-150 cm	4423	6916	7160	7397	13075	481

Geochemistry

There are trends in the concentration of some, but not all metals along the core at Koper 4 (figure 10). Several metals differ strongly in concentrations from the Po stations and Panzano, as well. The Zn concentration does not show any trend along the core at Koper 4. The Cr, Cu, and Ni concentrations increase in the upper part of the core, where they reach values similar to those in the upper part at Panzano. Concentrations of these metals are much higher in the middle to upper part at the Po stations, exceeding the NOAA ERL for Cr and Cu and the NOAA ERM for Ni. The Pb concentration strongly increases in the upper part at Koper 4, showing the same trend as at Panzano and attaining similar values as in the upper part at the Po stations. The highest Pb concentrations, however, are attained in the middle part of the Po stations, exceeding the NOAA ERL. The As concentration fluctuates strongly along the core at all stations. Unlike any other metal concentration, that of As attains the highest values at Koper 4 in the middle part, where it exceeds the NOAA ERL. The Cd concentration is stable for most of the lower and middle part at Koper 4, with some minor fluctuations in between, and increases in the upper part, but remains below concentrations observed at the other stations. Overall, metal concentrations are predominantly lower at Koper 4 compared to the other stations and often increase in the upper part of the core. Only the NOAA ERL for Ni and As is exceeded at Koper 4. The NOAA ERM is never exceeded at this station. For most metals, the highest concentrations are found at the Po stations.

TN and TOC show very similar trends along the core at Koper 4 (figure 10). They are comparatively high in the lower part and then decrease in the middle part, albeit with some minor reversals. In the uppermost 30 cm there is an increase in TN and TOC concentrations, albeit again with some minor reversals. At the top of the core similar concentrations as in the lower part are attained. TN and TOC concentrations increase upcore at the other stations. In the lower part of the studied cores the TN concentration is highest at Koper 4, but in the upper part higher values are attained at the other stations. The latter is also true for the TOC concentration, where the difference between Koper 4 and the other stations is even more pronounced.

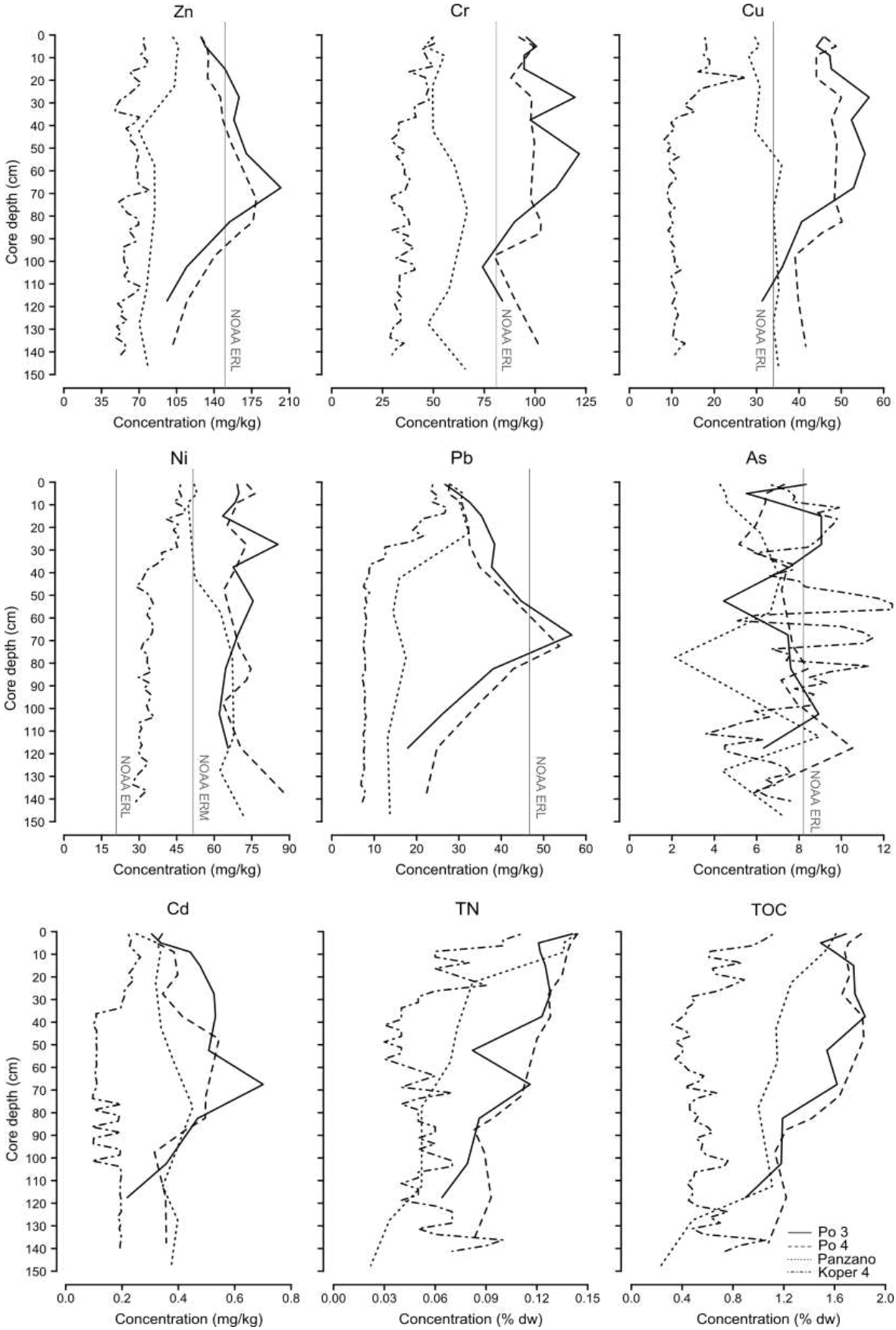

Figure 10. Trends of metal and nutrient concentrations along the cores from stations Po 3 (solid line), Po 4 (dashed line), Panzano (dotted line), and Koper 4 (dashed-dotted line). For metals, NOAA ERL or ERM is indicated, if its is exceeded by the concentration in at least on core. For Cd neither threshold level is indicated because concentrations remain below them throughout the cores at all stations.

Community composition

Shell density is lower in the TST-MFZ, remaining relatively constant around about 0.5 to 0.6 ind/cm^3, than in the HST of KOP4-21-10, where it reaches a maximum of more than 1.6 ind/cm^3 (figure 11). This can be explained by the higher proportion of sand and gravel, mostly composed of shells and biogenic debris, in the HST (see above). In the uppermost part of the HST, where the proportion of pelite increases again, shell density decreases. Raw species richness ranges from 40 to 63 and is lowest in the middle part of the core, where sample sizes are smaller as increments were split. Rarefied species richness ranges from 39 to 47 and changes only slightly along the core. It is highest in the lower part and decreases around the border between the TST-MFZ and the HST. The effective number of species, which varies from 12.6 to 18.0, is also higher in the TST.

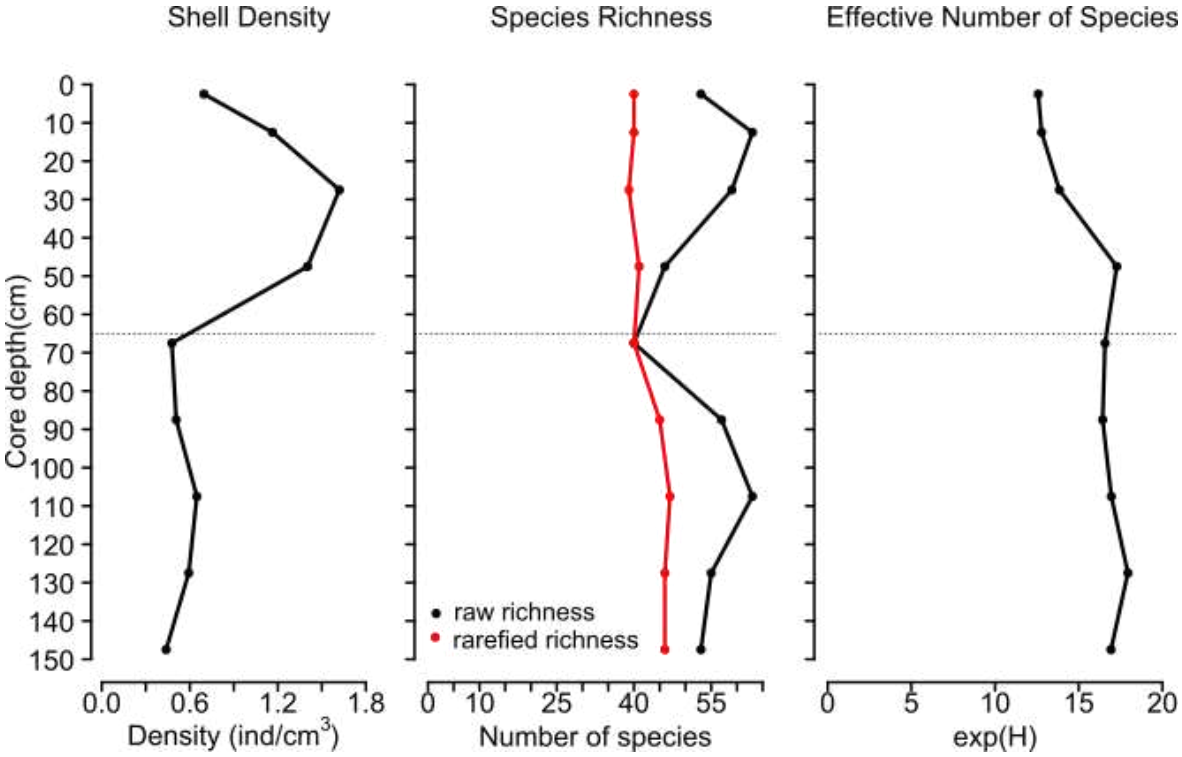

Figure 11. Trends in shell density (left), raw and rarefied species richness (middle), and effective number of species (right) along core KOP4-21-10 from station Koper 4.

NMDS based on relative species abundances indicates that community composition differs between the HST and the TST-MFZ, as increments from the respective units clearly separate along NMDS axis 1 (figure 12). PERMANOVA also indicates a significant difference in community composition between the two stratigraphic units (n_{perm} = 9999, F = 9.14, p = 0.0078).

V. gibba is the most abundant species in the core, followed by *T. tricarinata*. The relative abundance of *V. gibba* ranges from 25.5 to 36.8%, while that of *T. tricarinata* ranges from 4.9 to 10.9% (figure 13). The abundances of *V. gibba* and *T. tricarianta* change little relative to each other unlike at the other stations, where *V. gibba* increases and *T. tricarinata* declines in relative abundance in the upper

part of the cores (figure 13). Other species show more pronounced changes in abundance at Koper 4 (figure 14). *Gouldia minima* and *Nucula spp.* increase in abundance from the TST-MFZ to the HST. *Tritia varicosa*, *Ostrea edulis*, and *Abra nitida* decrease in relative abundance from TST-MFZ to the HST.

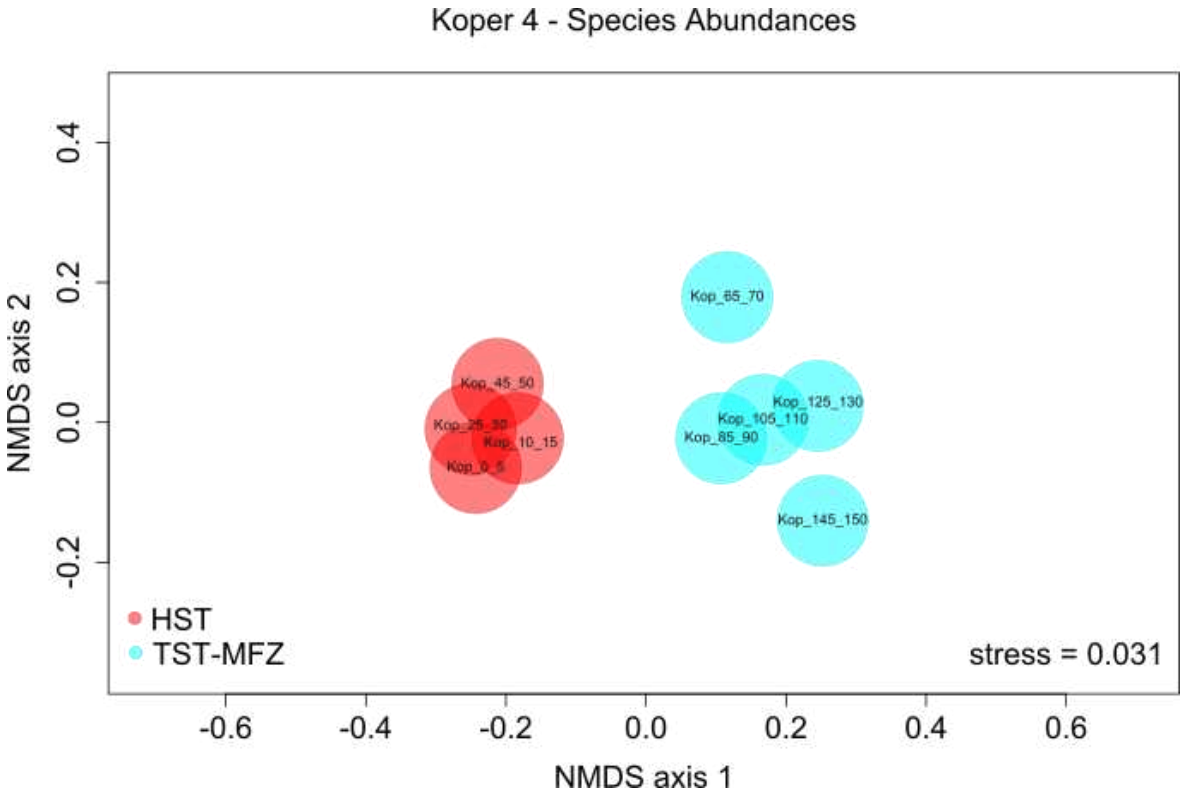

Figure 12. Two-dimensional NMDS for community composition based on square-root transformed relative abundance data from core KOP4-21-10 from station Koper 4.

Filter feeding is the dominant feeding guild throughout the core and shows a slight increase in relative abundance from 64% at the bottom to 80% at the top of the core (figure 15). Detritivores are the second most abundant feeding guild with more than 10% relative abundance in most increments. Scavengers, dominated by *Tritia varicosa*, have high relative abundances of more than 10% in the TST-MFZ, but decrease to 3 to 6% in the HST. Carnivores attain their highest relative abundances of almost 7% in the lower to middle HST. Among the most common carnivores are naticid gastropods, which can attain relative abundances of 4%. Relative abundances of these drilling predators are higher in the HST than in the TST-MFZ (figure 15).

Soft bottom infauna is the most abundant type of substrate relation. Its relative abundance ranges from 58 to 63% in the TST-MFZ unit and reaches more than 75% in the HST unit. The second and third most abundant substrate relations are specialized soft bottom infauna and infauna living on both, soft- and hard bottom, which reach relative abundances of more than 10% in most of the TST-MFZ. Their relative abundances are lower in the HST unit, which is also the case for specialized hard bottom epifauna. Throughout the core, more than 95% of the fauna does not have any vegetation association (figure 15).

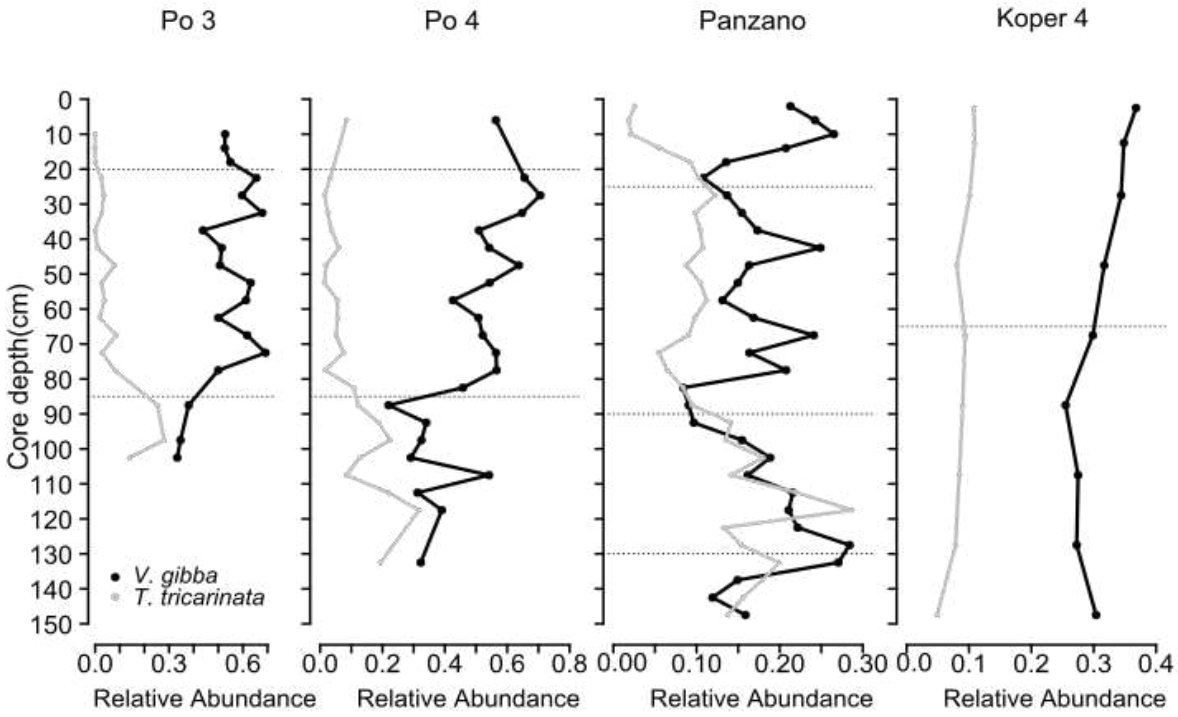

Figure 13. Trends in relative abundance of V. gibba *and* T. tricarinata *at all studied stations.*

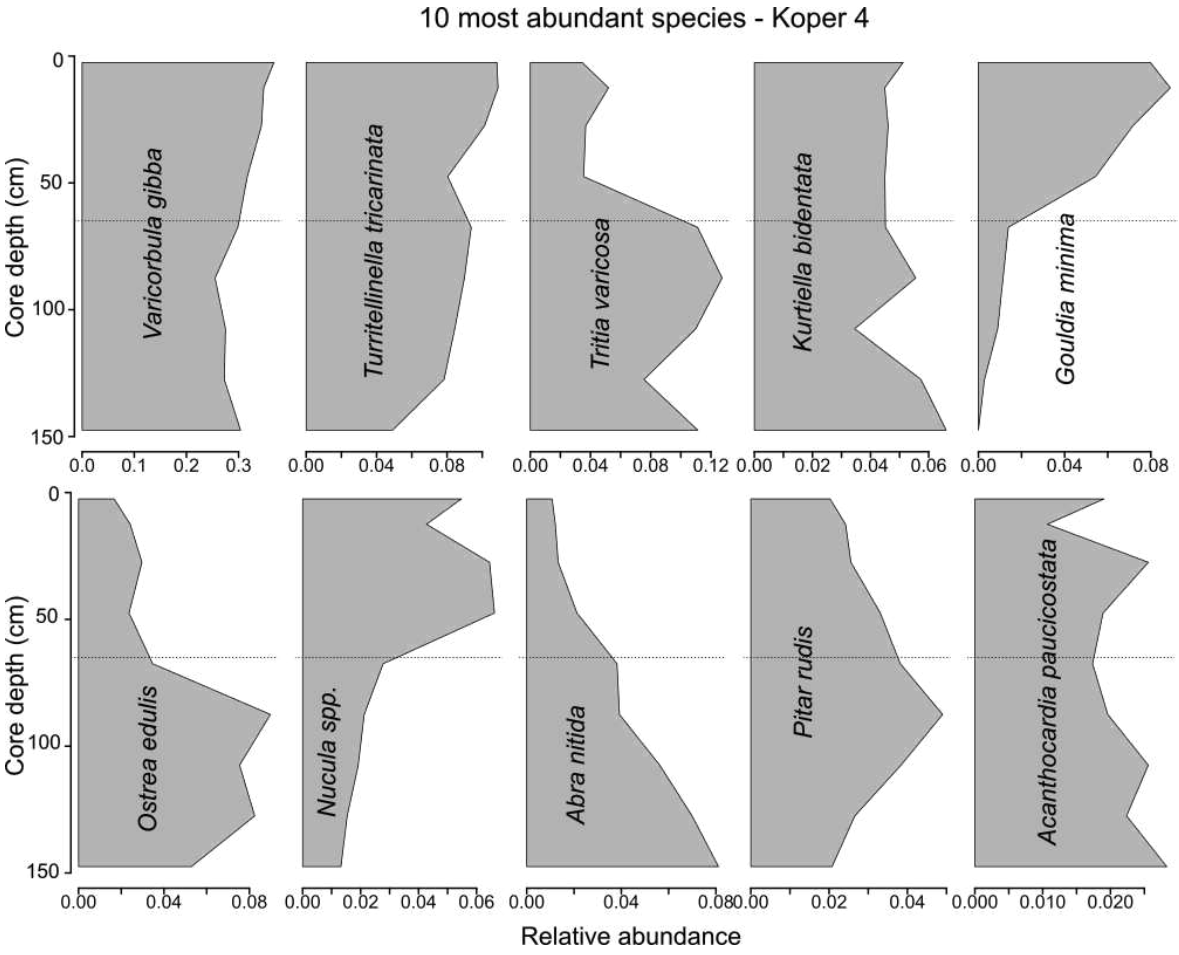

Figure 14. Trends in relative abundance of the ten most abundant species from core KOP4-21-10 from station Koper 4. Note the difference in scale between species.

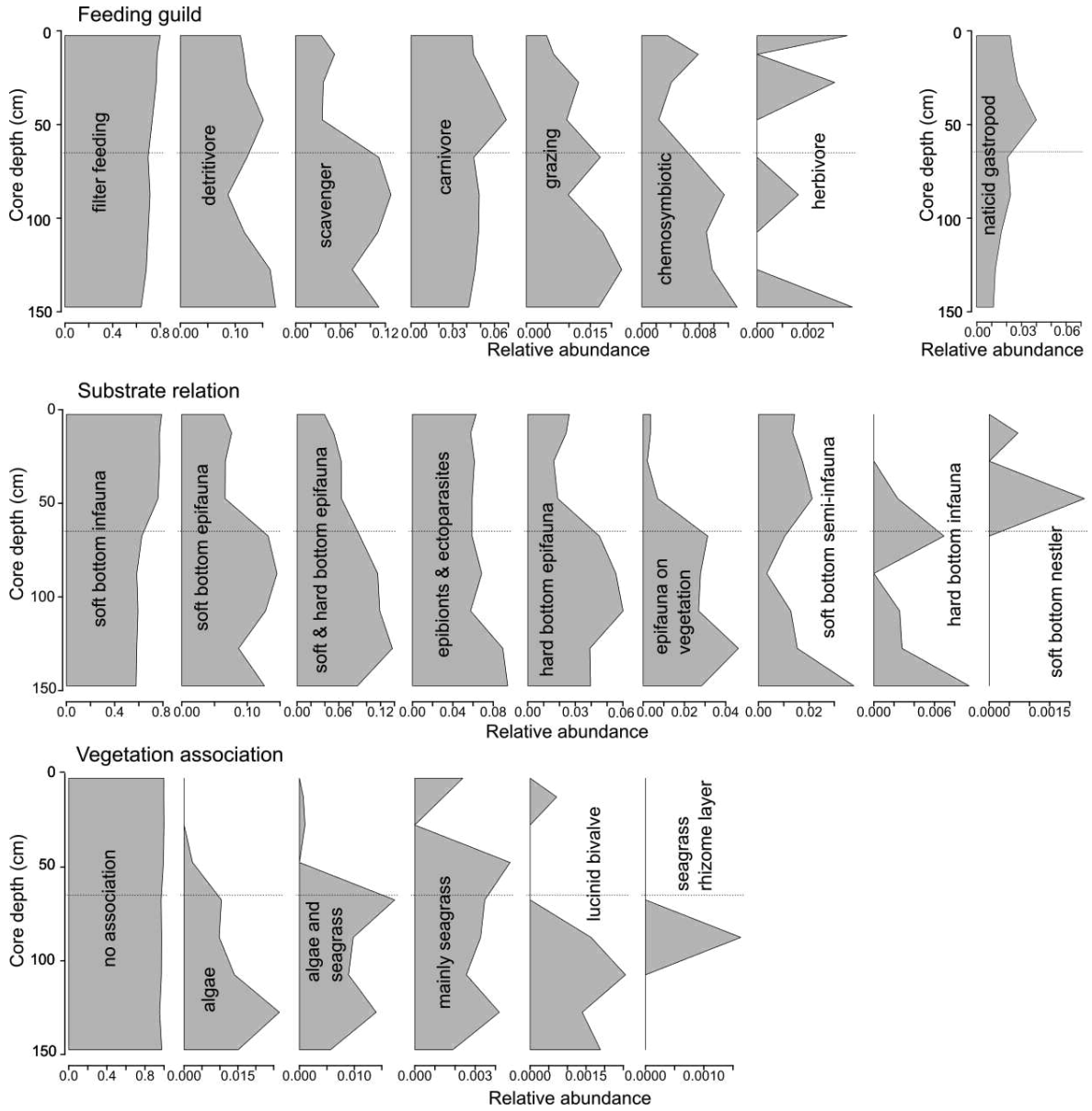

*Figure 15. Trends in relative abundance of feeding guilds, substrate relation, and vegetation association of mollusk communities from core KOP4-21-10 from station Koper 4. Note the difference in scale among ecological guilds. The relative abundance of naticid gastropods (*Euspira macilenta, Euspira nitida*), which belong to the carnivorous feeding guild, is also shown (topright).*

Size trends in the NAS

Size trends of *V. gibba* were previously studied for stations Po 3, Po 4 (Albano et al., 2018; Tomašových et al., 2020), and Panzano (Fuksi et al., 2018; Tomašových et al., 2020). They will also be discussed below to allow for a comparison with the size trends of *T. tricarinata* at the same stations.

Po 3

At station Po 3 *V. gibba,* increases in size from the lower part of the composite core, which can be assigned to the early 20th century based on shell ages (Tomašových et al., 2018), to the upper part which can be assigned to the late 20th and 21st century (figure 16). Median and 95th percentile sizes are generally highest

in the increments from the late 20th century, regularly exceeding 9 and 10 mm, respectively. This is reflected in very high frequencies of large size classes in the size distribution of the late 20th century (figure 17). The distributions from the late 20th and the 21st century are bimodal, unlike the right skewed, unimodal distribution of the early 20th century. Results of the Kruskal-Wallis test indicate statistically significant differences between the size distributions of the temporal units at Po 3 (χ^2 = 159.77, df = 2, p < 0.001). All pairwise comparisons of units by Wilcoxon rank-sum test were significant (table 5).

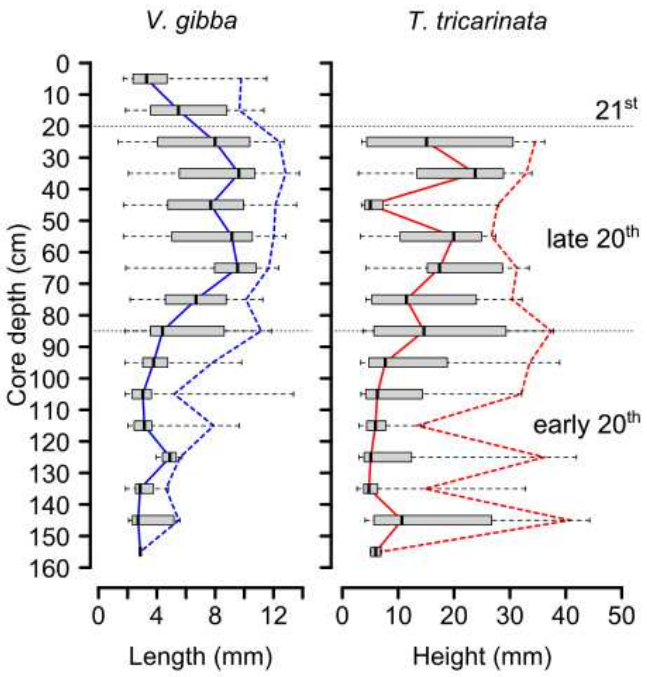

Figure 16. Size trends of V. gibba *(left) and* T. tricarinata *(right) at station Po 3. The solid line indicates the median, the dashed line the 95th percentile size.*

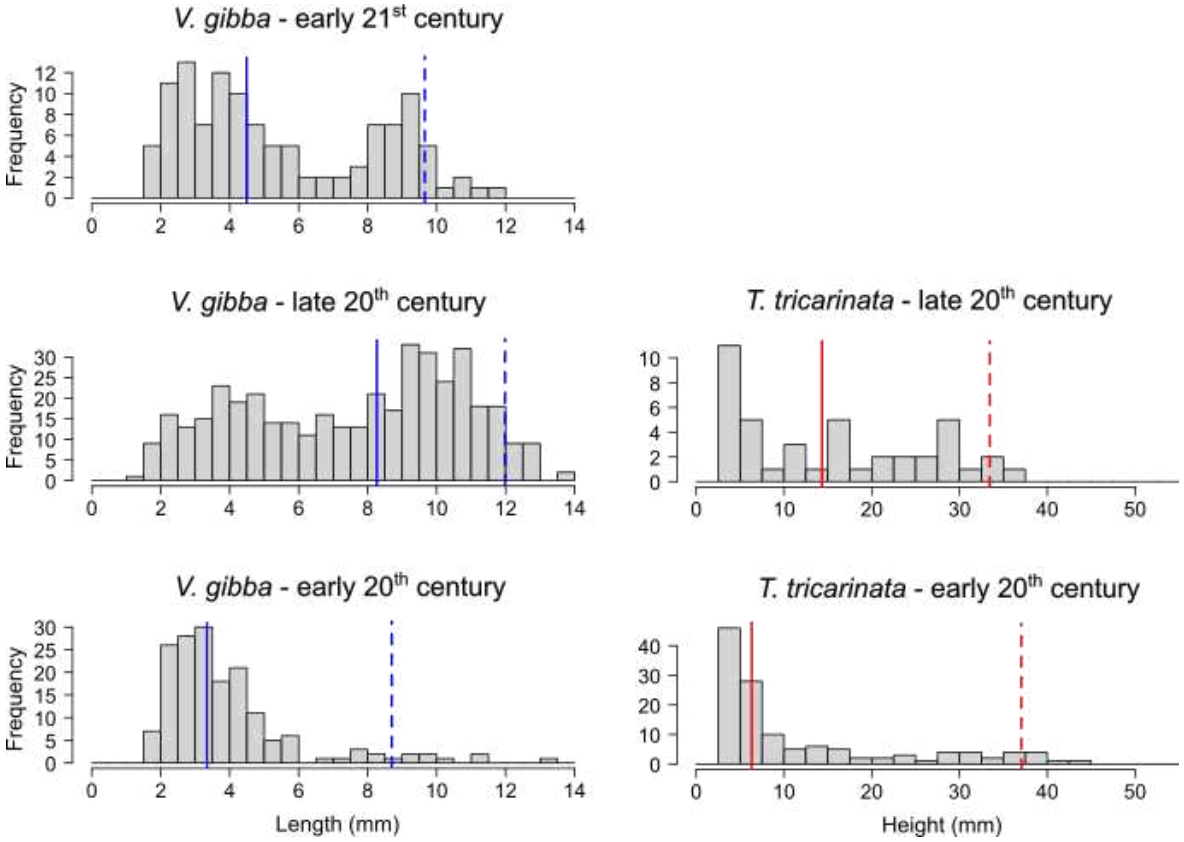

Figure 17. Size distributions of V. gibba *(left) and* T. tricarinata *(right) of the temporal units of station Po 3. The solid line indicates the median, the dashed line the 95th percentile size. Values for the median and 95th percentile size of the temporal units from all stations are summarized in the appendix.*

T. tricarinata also increases in size from the lower to the upper part of the core

(figure 16). The median size is generally higher in increments from the late- than from the early 20th century. Comparatively high 95th percentile sizes of 30 mm or more, however, are regularly found in both units. The size distribution of the early 20th century is right skewed, whereas that from the late 20th century is bimodal with higher relative frequencies of large size classes (figure 17). There are no measurable *T. tricarinata* specimens in increments from the 21st century. A Wilcoxon rank-sum test indicated that the difference between the size distributions from the early and late 20th century is not statistically significant (table 5).

Table 5. Wilcoxon rank-sum test statistic W and Bonferroni-corrected p-value for pairwise comparison of temporal units from station Po 3. Significant p-values are highlighted in bold.

	V. gibba		***T. tricarinata***	
	W	*p*	*W*	*p*
early vs. late 20th century	56643	**< 0.001**	3181.5	0.075
early 20th vs 21st century	13026	**< 0.001**	NA	NA
late 20th vs. 21st century	14916	**< 0.001**	NA	NA

Po 4

At station Po 4, *V. gibba* shows a similar upcore size increase as at Po 3. Among increments from the late 20th century, median and 95th percentile sizes are highest in the upper part from 20-60 cm depth, exceeding 9 and 11 mm, respectively (figure 18). Size decreases in the increments from the 21st century but remains at comparatively high values. The size distribution of the early 20th century is unimodal and right skewed. In contrast, the size distributions of the late 20th century and 21st century are bimodal and characterized by high frequencies of large size classes (figure 19). Results of the Kruskal-Wallis test indicate statistically significant differences between the size distributions of the temporal units at Po 4 (χ^2 = 124.5, *df* = 2, $p < 0.001$). All pairwise comparisons of units by Wilcoxon rank-sum test were significant (table 6).

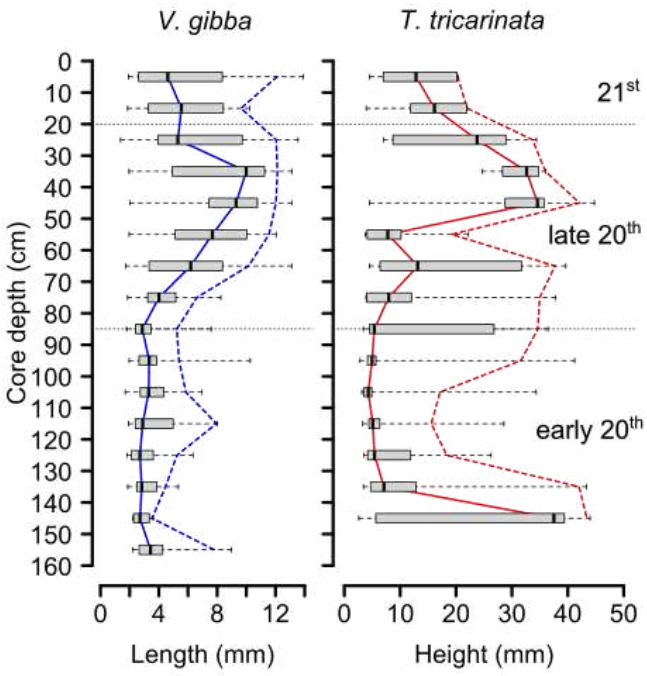

Figure 18. Size trends of V. gibba *(left) and* T. tricarinata *(right) at station Po 4. The solid line indicates the median, the dashed line the 95th percentile size.*

Table 6. Wilcoxon rank-sum test statistic W and Bonferroni-corrected p-value for pairwise comparison of temporal units from station Po 4. Significant p-values are highlighted in bold.

	V. gibba		***T. tricarinata***	
	W	*p*	*W*	*p*
early vs. late 20th century	71555.5	**< 0.001**	4516.5	**< 0.001**
early 20th vs 21st century	10213.5	**< 0.001**	854	0.052
late 20th vs. 21st century	23867	**0.014**	223	0.402

The median and 95th percentile size of *T. tricarinata* are generally higher for increments from the late- than from the early 20th century but also very high in the lowermost part of the core (figure 18). Size decreases again in the 21st century. The size distribution of the early 20th century is right skewed with low abundance of large individuals. The size distribution of the late 20th century is bimodal with comparatively high frequencies of large size classes. The size distribution of the 21st century is also bimodal but without any large specimens as the frequency peaks among small and middle size classes (figure 19). Results of the Kruskal-Wallis test indicate statistically significant differences between the size distributions of the chronologic units at Po 4 (χ^2 = 27.095, *df* = 2, $p < 0.001$). The pairwise comparisons by the Wilcoxon rank-sum test show that only the early and the late 20th century have significantly different size distributions (table 6).

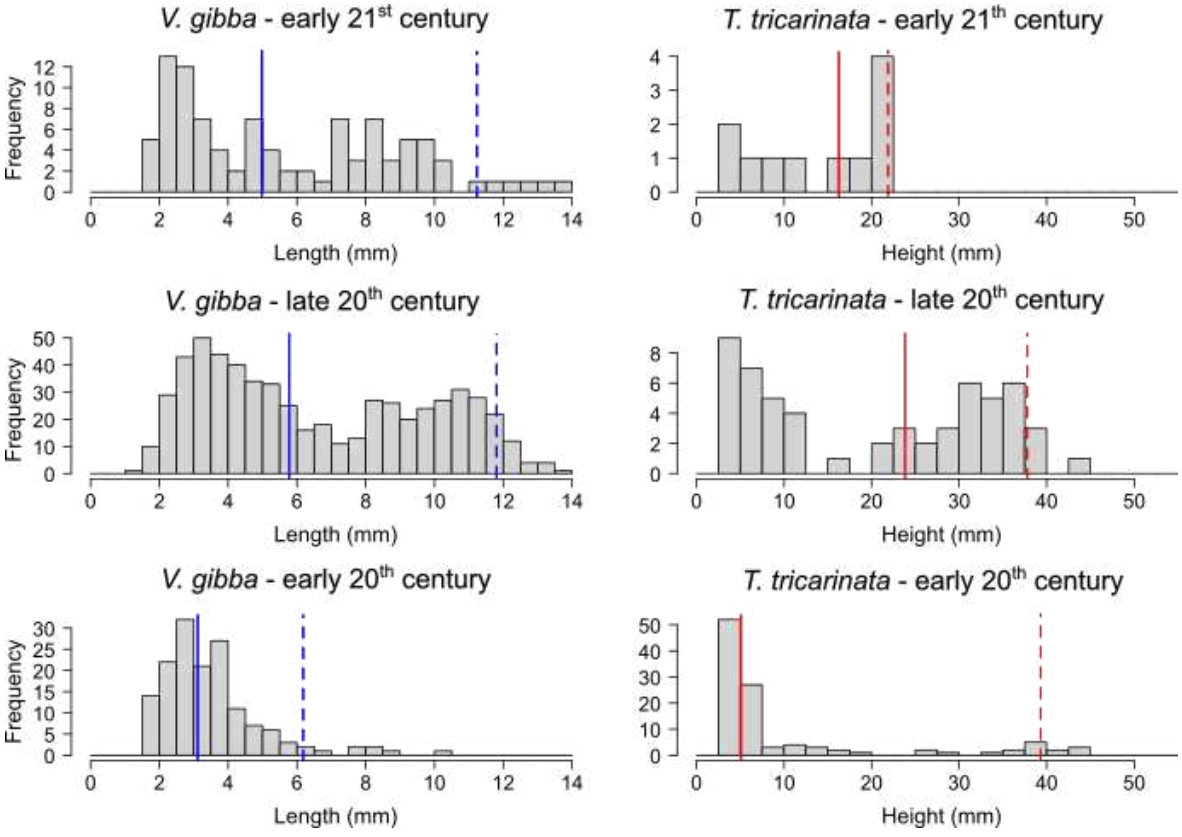

Figure 19. Size distributions of V. gibba *(left) and* T. tricarinata *(right) of the temporal units of station Po 4. The solid line indicates the median, the dashed line the 95th percentile size.*

Panzano

At station Panzano, size of *V. gibba* is stable in the lower and middle part of the composite core, which can be assigned to the 17th to 19th century based on shell ages (Tomašových et al., 2017). The median size is between 3 and 4 mm and the 95th percentile size fluctuates from 6 to 9 mm (figure 20). In the uppermost part, which can be assigned to the 20th and 21st century, the median size increases to around 4 mm and the 95th percentile size to more than 10 mm. The size distributions of the temporal units look very similar as they are all right skewed with a heavy tail as large size classes are moderately frequent (figure 21). This is most pronounced in the size distributions from the 20th and 21st century. Results of the Kruskal-Wallis test indicate statistically significant differences between the size distributions of the temporal units at Po 4 (χ^2 = 199.8, *df* = 3, p < 0.001). Pairwise comparison by the Wilcoxon rank-sum test indicates that the 20th to 21st century differs significantly in its size distribution from the 17th, 18th, and 19th century. The size distributions of the 18th and 19th century also differ significantly (table 7).

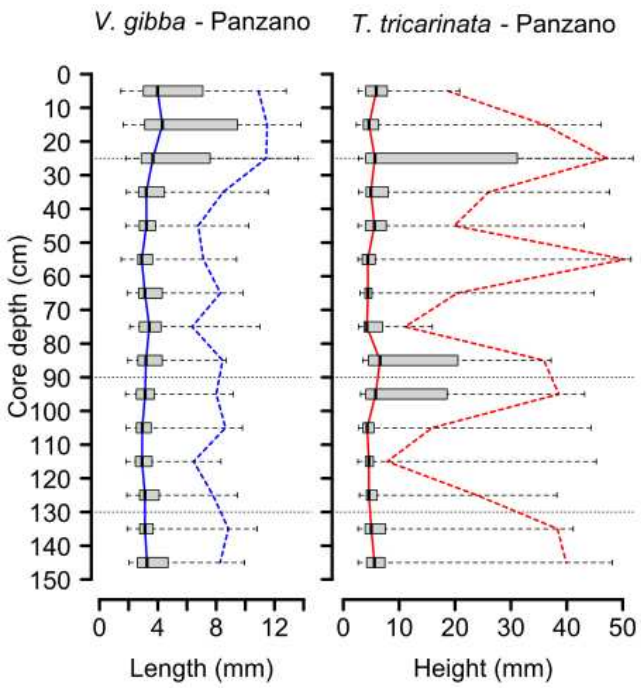

Figure 20. Size trends of V. gibba *(left) and* T. tricarinata *(right) at station Panzano. The solid line indicates the median, the dashed line the 95th percentile size.*

Table 7. Wilcoxon rank-sum test statistic W and Bonferroni-corrected p-value for pairwise comparison of temporal units from station Panzano. Significant p-values are highlighted in bold.

	V. gibba	
	W	*p*
17th vs. 18th century	54984	0.102
17th vs. 19th century	117969.5	1.000
17th vs. 20th and 21st century	125986	**< 0.001**
18th vs. 19th century	267103.5	**< 0.001**
18th vs. 20th and 21st century	275338	**< 0.001**
19th vs. 20th and 21st century	477382.5	**< 0.001**

The median size of *T. tricarinata* does not change much along the core, remaining around 5 mm (figure 20). The 95th percentile size, however, fluctuates strongly, ranging from less than 10 mm to more than 40 mm. In the lower part of the 20th to 21st century, high 95th percentile sizes are attained but they decrease towards the top of the core. This trend, however, fits within the range of size fluctuation seen

along the core. Size distributions are also right skewed with a heavy tail for all temporal units, although, as for *V. gibba*, the share of large specimens is most pronounced in the size distribution of the 20th to 21st century (figure 21). Results of the Kruskal-Wallis test do not indicate statistically significant differences between the size distributions of the temporal units at Panzano (χ^2 = 6.710, *df* = 3, *p* = 0.082).

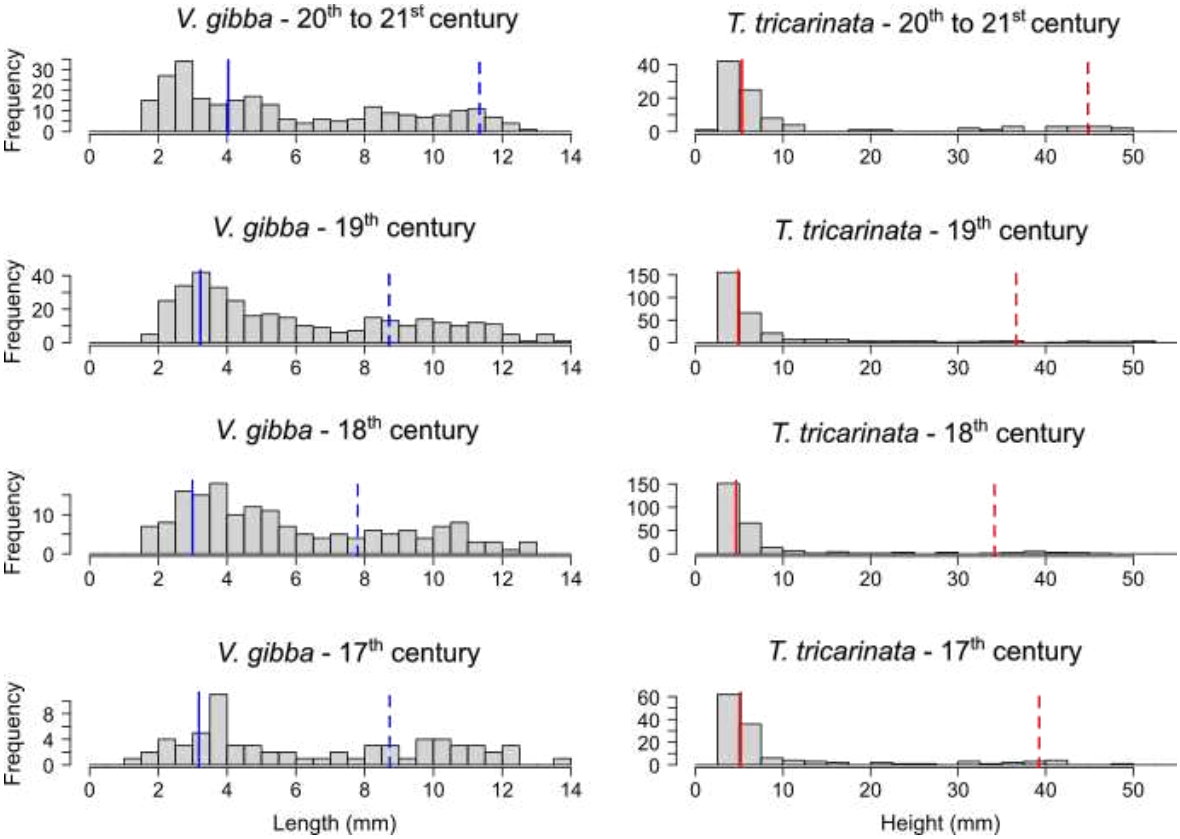

Figure 21. Size distributions of V. gibba *(left) and* T. tricarinata *(right) of the temporal units of station Panzano. The solid line indicates the median, the dashed line the 95th percentile size.*

Koper 4

At station Koper 4 the median size of *V. gibba* does not change much along the core, remaining between 3 and 4 mm (figure 22). The 95th percentile size remains relatively stable within the stratigraphic units but is generally lower in the TST-MFZ, fluctuating around 8 mm, than in the HST, where it ranges mostly from 9 to 10 mm. The size distributions of both units are right skewed and unimodal but with a heavy tail in the HST, in which larger size classes are more frequent (figure 23). Results of the Wilcoxon rank-sum test indicate a statistically significant difference between the size distributions of the two units (W = 3806503, $p < 0.001$).

Compared to *V. gibba*, the median size of *T. tricarinata* varies more, being high in the lowermost part of the core, reaching values of more than 10 mm in some increments (figure 22). The median size is lower in the middle and upper part of the TST-MFZ, then increases again, reaching values of almost 20 mm in the lower HST. In the middle to upper part of the HST the median size is generally the lowest

along the core. The trend for 95th percentile size is similar but with more pronounced fluctuations, as it ranges from less than 10 mm to almost 50 mm along the core. The size distributions of both stratigraphic units are right skewed and unimodal, although that of the HST has a heavier tail (figure 23). Results of the Wilcoxon rank-sum test indicate a statistically significant difference between the size distributions of the two units ($W = 79331$, $p < 0.001$).

Table 8. Spearman's rank correlation for fragmentation and shell density, median, and 95th percentile size of V. gibba *and* T. tricarinata *along core KOP4-21-10 from station Koper 4. Significant p-values are highlighted in bold.*

	V. gibba			***T. tricarinata***		
	ρ	*S*	*p*	*ρ*	*S*	*p*
Fragmentation vs. density	0.19	5301.6	0.282	0.78	1447.1	**< 0.001**
Fragmentation vs. median size	-0.12	7350.2	0.488	-0.62	10632	**< 0.001**
Fragmentation vs. 95th percentile size	0.12	5745.8	0.492	-0.44	9442	**0.009**

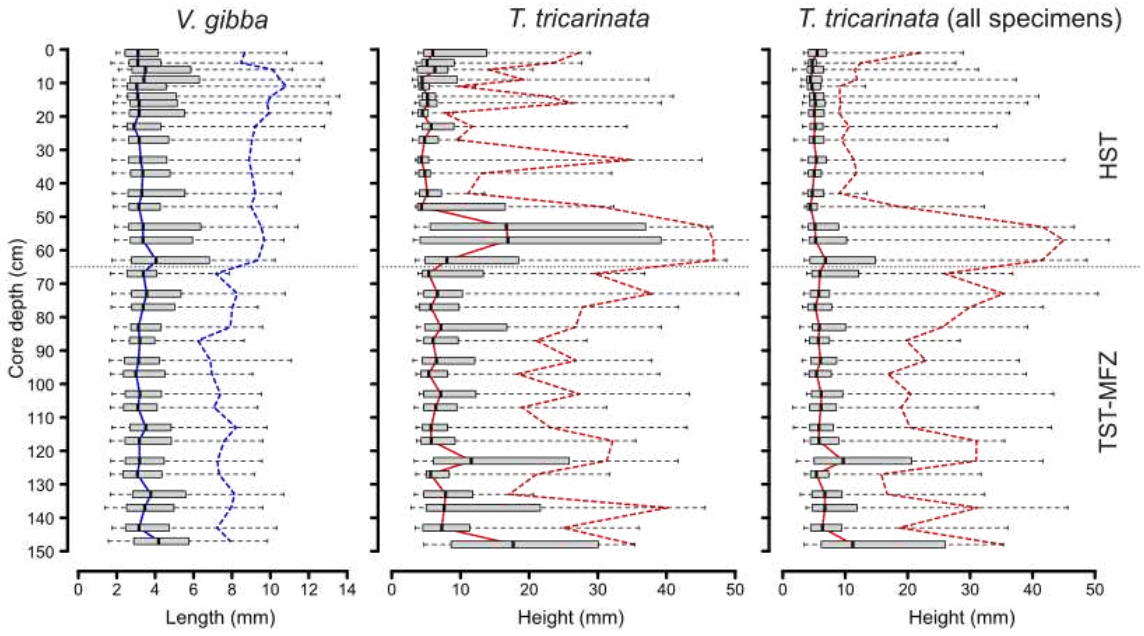

Figure 22. Size trends of V. gibba *(left),* T. tricarinata *without specimens of fragmentation score 1 (middle), and of* T. tricarinata *based on all specimens including those with fragmentation score 1 (right). The solid line indicates the median, the dashed line the 95th percentile size. Size trends of* T. tricarinata *discussed in the text are based on the dataset without specimens of fragmentation score 1. The trend of the dataset with such specimens is shown for comparison. Note the similarity in trends between the two.*

A large proportion of *T. tricarinata* specimens from Koper 4 was not used for the size analysis as they were too fragmented (fragmentation score 1). For *V. gibba*, this was not the case as highly fragmented specimens never make up more than 15% of the specimens in an increment (figure 24). For *T. tricarinata*, on the other hand, more than 80% of the specimens from some increments were excluded from the size analysis. Furthermore, there is a clear trend in the proportion of highly

fragmented specimens, which is much lower in the TST-MFZ than in the HST. For *T. tricarinata*, the proportion of fragmented specimens is significantly positively correlated with the density of individuals (in ind/cm^3), but significantly negatively correlated with its median size. For *V. gibba*, there is no significant correlation between the fragmentation and either density, median, or 95th percentile size (table 8). The general pattern of *T. tricarinata* reaching larger sizes in the TST-MFZ, maximum size in the lower part of the HST and otherwise smaller sizes in the upper HST remains the same, when highly fragmented specimens are included (figure 22).

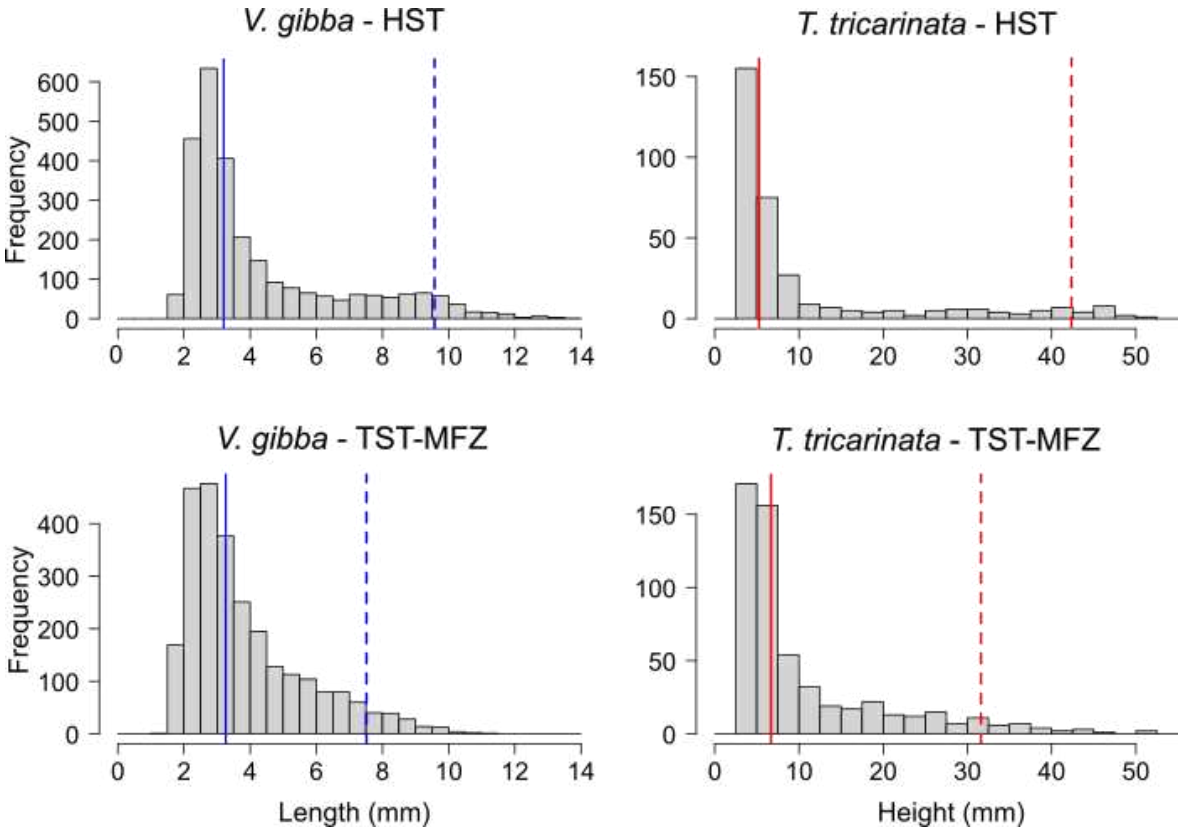

Figure 23. Size distribution of V. gibba *(left) and* T. tricarinata *(right) of the stratigraphic units of station Koper 4. The solid line indicates the median, the dashed line the 95th percentile size.*

NMDS of size distributions

For *V. gibba* there is a temporal separation of groups of samples along NMDS axis 1 (figure 25). There are two clusters with negative NMDS axis 1 scores that comprise the late 20th and 21st century increments from the Po stations and Panzano, which are characterized by bimodal size distributions with high relative frequencies of large size classes (figures 17, 19, 21). In contrast, the early 20th century increments from these stations and increments from Koper 4, which can be assigned to the 20th to 21st century based on ^{210}Pb activity (see results above), have higher NMDS axis 1 scores and group together with increments assigned to the pre-20th century HST or TST-MFZ. This cluster represents increments with unimodal, right skewed size distributions (figures 17, 19, 21; size distributions for 5-cm-increments from Koper 4 are shown in the appendix). Within this cluster, the

early 20th century increments from the Po stations tend to have the highest NMDS axis 1 scores. Increments from the pre-20th century HST tend to have lower NMDS axis 1 scores than those from the TST-MFZ. Among HST increments those from Koper 4 tend to have lower scores than those from Panzano.

For *T. tricarinata* there is no clear temporal separation of the increments (figure 26). The two late 20th century increments from the Po stations, which are characterized by high relative frequencies of large size classes (figures 17, 19), have very low NMDS axis 1 scores, albeit very different NMDS axis 2 scores. Other 20th and 21st century increments cluster with increments from before the 20th century. Most of the increments from the pre-20th century HST and the TST-MFZ have positive NMDS axis 1 scores. Exceptions are the increments from the lower parts of the HST and the TST-MFZ of station Koper 4 which are characterized by comparatively high relative frequencies of middle to large size classes (see appendix). Increments from the HST tend to have higher NMDS axis 2 scores than those from the TST-MFZ, which could be because of comparatively low relative frequencies of middle size classes in the HST.

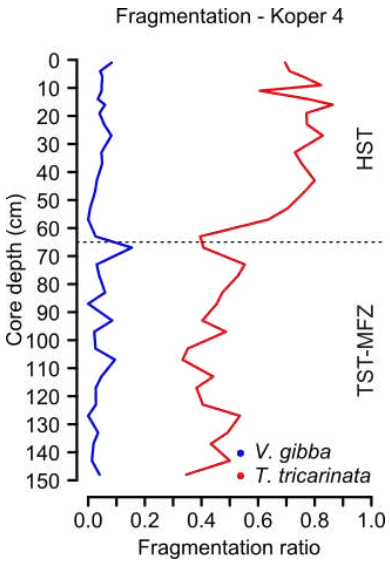

Figure 24. Trends in the proportion of highly fragmented specimens (fragmentation score 1, not used for size analysis) along core KOP4-21-10 from station Koper 4.

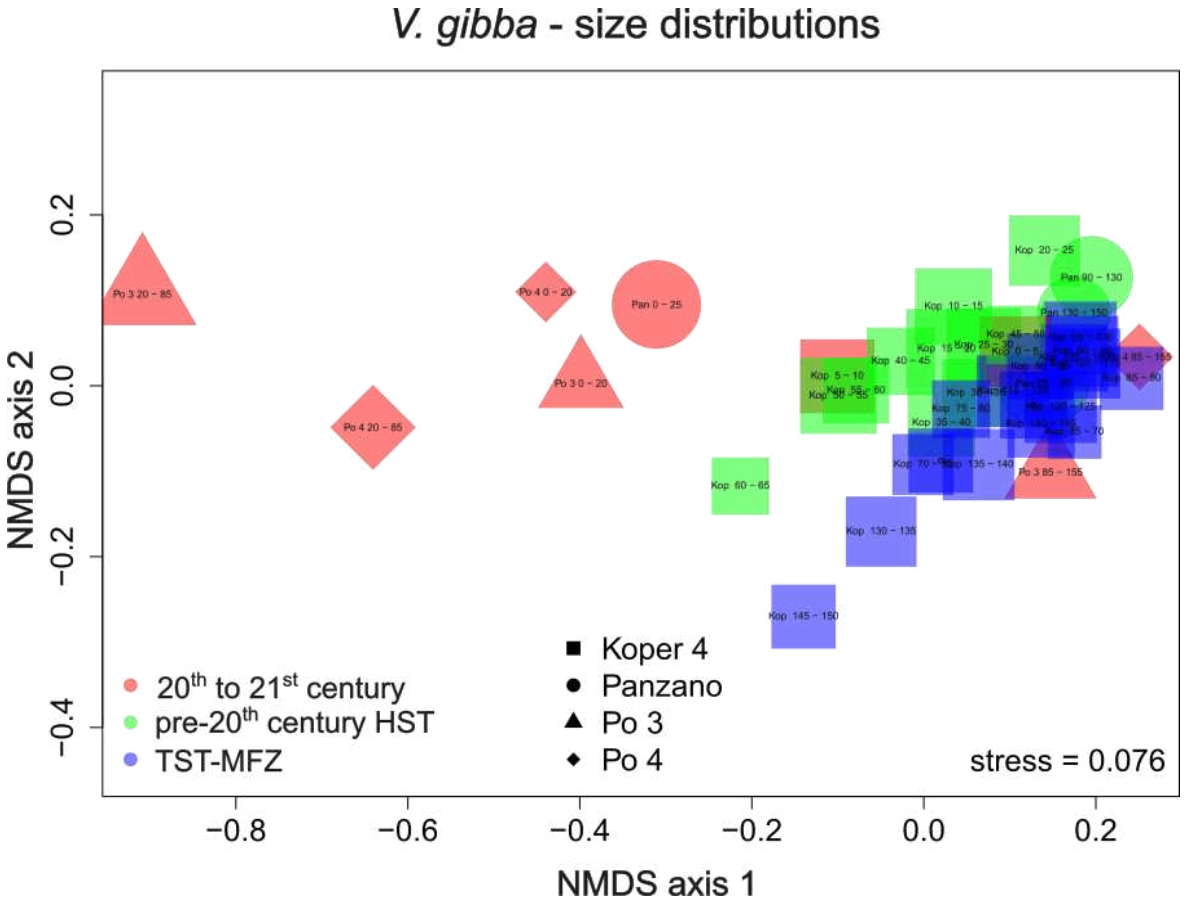

Figure 25. Two-dimensional NMDS for size distributions of V. gibba *based on Kolmogorov distances Sizes of the symbols are proportional to the natural logarithm of the sample sizes of the core intervals they represent.*

Discussion

Long-term trends at Koper 4

Radiocarbon dating of shells revealed that the record at Koper 4 is well suited to study long-term trends in size as it goes back to the upper part of the TST of the Holocene transgression. Interestingly, the interquartile ranges of the age distributions of *V. gibba* are higher for the HST than for the TST-MFZ. Interquartile age ranges are commonly used as indicator of the degree of time averaging (Kidwell, 2013; Krause et al., 2010; Nawrot et al., 2022). Higher time averaging could be the result of lower sedimentation rates in the HST. The average sedimentation rate for the entire core calculated from shell dating is 0.21 mm/year. For the HST and TST-MFZ sedimentation rates of 0.10 mm/year and 0.73 mm/year, respectively, were calculated. Lower sedimentation rates for the HST would differ from the pattern seen in the western NAS (Amorosi et al., 2017) but have already been found in other sites located in the eastern parts of the basin, for example outside of Piran Bay located in the Gulf of Trieste west of Koper Bay (Gallmetzer et al., 2019; Tomašových et al., 2019). This has been related to the onset of modern circulation patterns in the NAS during the time of maximum flooding (Asioli et al., 1996; Piva et al., 2008), which lead to the winnowing of fine particles (Gallmetzer et al., 2019). This could explain the higher proportion of coarser grain size fractions in the HST at Koper 4.

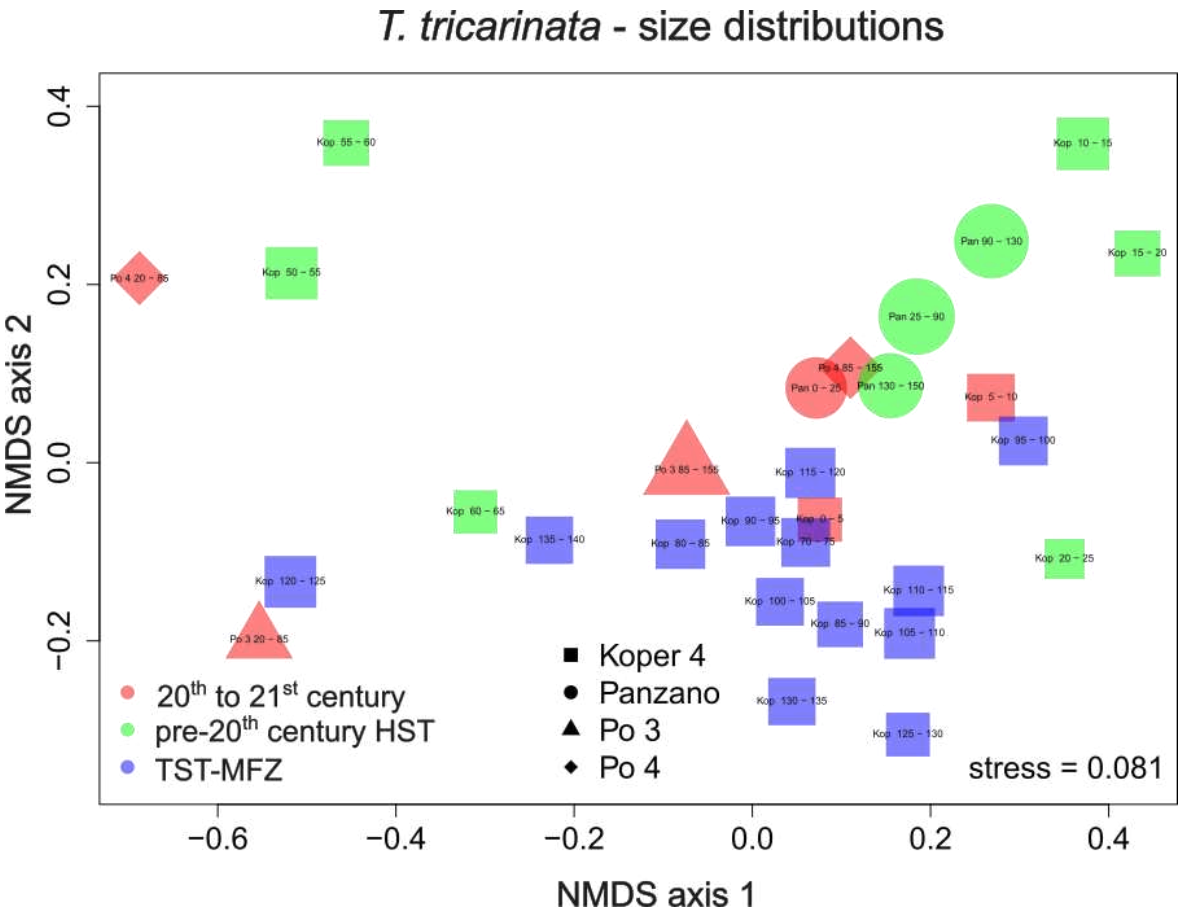

Figure 26. Two-dimensional NMDS for size distributions of T. tricarinata *based on Kolmogorov distances. Sizes of the symbols are proportional to the natural logarithm of the sample sizes of the core intervals they represent.*

The results of ^{210}Pb dating indicate a sedimentation rate of 0.39 mm/year for the uppermost part of the HST, which are higher than the average rate calculated for the HST based on shell ages. Results of ^{210}Pb dating should be interpreted with caution, however, because it is based on very few data points and high ^{210}Pb excess values in lower parts of the HST demonstrate the impact of bioturbation in this condensed core. Contradictions in sedimentation rate estimates based on shell dating and ^{210}Pb dating were also found in other studies on highly condensed cores (Gallmetzer et al, 2019). This can be the result of sediment mixing which can lead to an overestimation of sedimentation rate based on ^{210}Pb dating (Johannessen and Macdonald, 2012). The higher sedimentation rate for the uppermost part of the HST could, however, be a true ecological signal as sediment loads in the Adriatic Sea increased during the last millennia because of deforestation and wetland reclamation during the Roman and Medieval periods (Lotze et al., 2011). This could also be the cause for the increase in pelite in the uppermost part of the HST. Similar trends of sediment siltation have been observed in other cores from the eastern NAS (Gallmetzer et al., 2019)

The uppermost part of the HST is also characterized by a decrease in shell density compared to the rest of the HST. The very high shell densities in most of the HST are probably the result of stratigraphic condensation and thus higher time averaging. Interestingly, rarefied species richness and the effective number of species are lower in the HST despite higher time averaging, albeit only slightly. Community composition and ecological guilds differ between the HST and the TST-MFZ. One potential driver is the change in sediment composition. For example, *G. minima*, a species preferring sandy substrates (Tomašových et al., 2019), has a higher abundance in the HST characterized by coarser sediment. The consistently high relative abundances of *T. tricarinata* and *V. gibba* can be explained by pelite remaining the dominant grain size fraction throughout as both species prefer finer substrates (Allmon, 1988; Hrs-Brenko, 2006).

Although *T. tricarinata* and *V. gibba* do not change much in relative abundance at Koper 4, they show changes in size. The 95th percentile size of *V. gibba* is higher for the HST than for the TST-MFZ. This results in a heavy-tailed size distribution for the HST. Such unimodal distributions with an increased share of larger specimens were previously found for *V. gibba* in the upper HST of condensed cores (Fuksi et al., 2018; Tomašových et al., 2020). Tomašových et al. (2020) found that size distributions become bimodal, like those from the late 20th and 21st century at Panzano and the Po stations, when only young shells with preserved periostracum were included. Thus, unimodal, heavy-tailed distributions resulted from time averaging due to mixing of younger death assemblages characterized by bimodal size distributions with older death assemblages with unimodal, right skewed size distributions. A similar mechanism can explain size patterns in the HST at Koper 4.

As mentioned above, the modern circulation pattern of the NAS started around the time of maximum flooding (Asioli et al., 1996; Piva et al., 2008). The modern circulation pattern regularly leads to water stratification in the Gulf of Trieste during summer, which can result in hypoxic events (Kralj et al., 2019; Ogorelec et al., 1991). Although the frequency of hypoxic events was increased by anthropogenic eutrophication during the late 20th century (Justić, 1991), hypoxic events are a natural phenomenon in the Gulf of Trieste and other parts of the NAS. Climate change during the Holocene lead to changes in water temperatures and river run-off, which affect the tendency to stratification and thus the frequency of hypoxic events. During the centuries preceding the 20th century this caused natural changes in the relative abundance of *V. gibba* in the Gulf of Trieste (Tomašových et al., 2017). Given that the current oceanic regime of the NAS was present throughout the highstand phase of the Holocene, it is possible that phases of high hypoxia frequency occurred throughout this time. During such phases *V. gibba* would have increased in relative abundance and in size. Time averaging of such populations with those living at times of low hypoxia frequency could have resulted in the size distributions found in the HST at Koper 4.

Recurring phases of high hypoxia frequency could also explain the decrease in relative abundance of epifaunal species, such as *O. edulis*, at Koper 4. This differs from the trend of other sites in the Gulf of Trieste like those located outside of Piran Bay, where the MFZ and early HST are characterized by the presence of *Arca-Ostrea* banks (Gallmetzer et al., 2019; Mautner et al., 2018). The Piran sites are located further offshore, however, and thus not as close to a source of riverine nutrient input as Koper 4. The difference between sites could also indicate that hypoxic events had a smaller spatial extent throughout most of the highstand phase compared to the late 20th century.

Unlike *V. gibba*, *T. tricarinata* is smaller in most of the HST than in the TST-MFZ at Koper 4. It is unlikely that this resulted from recurring phases of high hypoxia frequency for two reasons: 1) it is doubtful that *T. tricarinata* consistently responds with a size decrease to hypoxic events (see discussion below) and 2) as *T. tricarinata* becomes rare in response to hypoxic events, the size distributions of highly time-averaged death assemblages will be strongly dominated by the size classes that are prevalent during times of low hypoxia frequency when *T. tricarinata* is abundant.

A possible explanation for the decrease in size in the HST is the increase in drilling predation during the highstand phase in the NAS (Zuschin et al., 2022). At Koper 4 the relative abundance of naticids increases in the HST. These shell-drilling gastropods commonly prey on turritellids (Hagadorn and Boyajian, 1997; Tull and Böhning-Gaese, 1993) *V. gibba* is also regularly attacked but conchiolin layers in its shell make it less susceptible than other species (Kardon, 1998). Increased predation of *T. tricarinata* would lead to less survival into adulthood and thus result in smaller size in the HST. Changes in drilling frequency at the other studied

stations contradict this conclusion, however. Drilling frequencies are high in the mid-20th century but decline during the late 20th century due to anthropogenic impacts at the Po stations and Panzano (Zuschin et al., in press). Sizes of *T. tricarinata* are high from the mid- to the late 20th century at the Po stations and decline during the late 20th century at Panzano. Thus, there is no consistent association of high rates of drilling predation and small sizes of *T. tricarinata*. On the other hand, there are other potential drivers of size changes of *T. tricarinata* at the Po stations and Panzano (see discussion below). Consequently, an increase in drilling predations during the HST cannot be ruled out as an explanation for the observed size decrease of *T. tricarinata* at Koper 4.

Another potential driver of size changes in *T. tricarinata* are changes in nutrient input. TN and TOC concentrations decline from the lower to the middle-upper part of the core at Koper 4 and thus from the TST-MFZ to the lower HST. This decline could be the result of lower riverine input as water depth increased from the trangressive phase to the time of maximum flooding (Vacchi et al., 2016) and the successive onset of the modern circulation patterns of the NAS (Asioli et al., 1996; Piva et al., 2008) which entail the influx of warm, oligotrophic waters from the South (Giani et al., 2012; McKinney, 2007). The growth rate of some suspension feeding mollusks is positively correlated with productivity (Carmichael et al., 2012). Therefore, lower nutrient concentrations could have led to smaller sizes of *T. tricarinata* in the HST.

Trends in nutrient concentrations and size of *T. tricarinata* do not parallel each other throughout the core, however. TN and TOC concentrations increase again in the uppermost 30 cm, whereas size increases only in the uppermost 10 cm. Increases in nutrient concentrations and consequently size in the upper 10 cm could be related to eutrophication by increased fertilizer input during the 20th century (Justić, 1991). Small sizes from 10-30 cm depth could be the result mixing of the younger, often large shells with older, predominantly small shells from greater depths. Thus, the discrepancy between small sizes and high nutrients concentrations would be an artefact of time averaging of death assemblages. However, if it is a true ecological signal, the causal relationship between size and nutrient concentrations might not be very strong or other factors such as drilling predation are equally or more important in determining the size structure of *T. tricarinata*.

Although the size of *T. tricarinata* is generally lower in the HST, there are exceptions. In the lowermost parts of the HST this species is very large, but only in two increments. As the record at Koper 4 is only based on one core, unlike for the other stations for which composites of multiple cores were used, local sedimentary processes could be an explanation for this interval characterized by large size. Storms and other high energy events can result in size sorting of shells (Menard and Boucot, 1951; Zuschin et al., 2005). Given the low sedimentation rates in the HST at Koper 4, shells were exposed very long on the seafloor and thus surely

subjected to multiple high energy events. In the absence of any plausible environmental driver, such a taphonomic explanation for the large size of *T. tricarinata* in this interval appears to be a good alternative.

Lower sedimentation rates and higher time averaging in the HST are probably also the reason for the large share of highly fragmented shells of *T. tricarinata*. As a result of higher proportions in the HST, more specimens were excluded for size analysis from HST than from TST-MFZ increments. This did not affect size trends, however. If anything, the pattern of smaller size in the HST than in the TST-MFZ is even more pronounced if highly fragmented shells are included. Thus, the results of the size analysis are robust against the influence of fragmentation. That size trends remain similar if highly fragmented specimens are included has also important implications for future studies. If well-preserved specimens are very rare, fragmented specimens providing minimum size estimates could be included in size analysis to increase sample size.

Size response to anthropogenic stressors in the NAS

Using the same data as previous authors (Albano et al., 2018; Fuksi et al., 2018; Tomašových et al., 2020) I was able to replicate their results, which demonstrate an increase in size of *V. gibba* during the late 20th century. Higher growth rates resulting from eutrophication, as well as higher survival rates because of competitive and predator release in response to high hypoxia frequency have both been invoked as drivers of this trend (Fuksi et al., 2018; Tomašových et al., 2020). I consider it plausible that both drivers played a role. The bimodal size distributions with very high relative frequencies of large size classes point to a higher survival rate which could have resulted from competitive and predatory release. Nutrient input could have also played a role as indicated by the larger average sizes that were attained at the Po stations, which are located in the eutrophic western NAS (Zavatarelli et al., 1998), compared to Panzano and Koper 4.

Unlike *V. gibba*, *T. tricarinata* does not show a uniform size response to the anthropogenic stressors of the late 20th century. At the two Po stations size increased during the late 20th century despite population declines. At Panzano, on the other hand, size decreased during the 20th century although the magnitude of this shift does not stand out compared to fluctuations in size during previous centuries.

Size increases of *T. tricarianta* during the late 20th century at the Po stations might have had two drivers: 1) eutrophication could have led to higher growth rates (see discussion above), and 2) less recruitment of juveniles could have led to a higher proportion of large-sized adults. The latter was used to explain a size increase despite a population decline in the deposit feeding bivalve *Nucula annulata* in environments characterized by eutrophication and recurring hypoxic events (Craig, 1994). *T. tricarinata* tends to aggregate in large numbers during reproduction and males directly transfer spermatophores to females (Allmon, 2011). It has been

proposed that this mode of reproduction might lead to an Allee effect, resulting in recruitment failure when populations decline (Shin et al., 2020). As *T. tricarinata* populations declined in response to high hypoxia frequency, recruitment failure might have led to populations dominated by large-sized adults.

Population declines also occurred at Panzano but here size decreased during the 20th century. Although lower recruitment might have led to adult-dominated populations at the Po stations, there is no reason to believe that such populations resulted from higher mortality of juveniles during hypoxic events. In fact, studies on other mollusks suggest a higher vulnerability of larger individuals to hypoxia (Altieri and Witman, 2006; Clark et al., 2013). Thus, larger individuals of *T. tricarinata* were surely severely affected by hypoxic events at Panzano during the late 20th century. There might have been recurring local extirpations of the population at Panzano and the death assemblages from the late 20th century could have resulted from multiple unsuccessful reestablishment attempts of juveniles which were time averaged.

The different fate of *T. tricarinata* populations from the Po stations and Panzano might be the result of stochastic events, as there is no plausible driver of this difference. The stations are similar in their histories of eutrophication and increased hypoxia frequency during the late 20th century (Tomašových et al., 2018). Concentrations of most pollutants are higher at the Po stations than at Panzano. Ni is the only studied pollutant that exceeds the NOAA ERM, above which effects on benthic organisms are likely to occur, at Panzano but its concentration is highest in the record from the 17th to 19th century. Panzano has a very high Hg concentration, exceeding the NOAA ERM throughout, but concentrations were also lower during the 20th century than before (Gallmetzer et al., 2017; Vidović et al., 2016). Thus, metal pollution is not a plausible driver of population decline at Panzano. Apart from the lack of other potential drivers, a stochastic explanation of differences between sites also fits well with the ecology of turritellids which have strong population fluctuations, which might be due to stochastic larval settlement (Shin et al., 2020).

The comparison of size distributions across the four stations, indicates that the bimodal size distributions of *V. gibba* developed in response to the anthropogenic stressors of the late 20th century are unique in the context of the Holocene fossil record of this species. Tomašových et al. (2020) even referred to trends in abundance and size of *V. gibba* during the 20th century as a regime shift. In contrast, the size response of *T. tricarinata* during the 20th century was not uniform. Size distributions of the late 20th century from the Po stations are characterized by a high proportion of middle- to large-sized specimens. Such size distributions are also found in the lower parts of the HST and TST-MFZ at Koper 4 but the former might be attributable to sedimentary size sorting instead of ecological processes (see discussion above). Size distributions from Panzano, on the other hand, are dominated by small-sized individuals like most samples of this

species from the Holocene in the NAS.

Before regime shifts are invoked, one must also consider the difference in time averaging between the core intervals that were compared. Core intervals from the Po stations and Panzano represent (half-)centuries and time averaging is on the scale of decades at the Po stations (Tomašových et al., 2018), and centuries at Panzano (Tomašových et al., 2017). In contrast, time averaging of individual increments at Koper 4 can be more than 2000 years. If core intervals from the 20th century of the Po stations and Panzano were pooled with those from previous centuries, it would result in samples with age distributions that are more comparable to increments from Koper 4. Such samples would probably have unimodal, right skewed size distributions, but with a heavy tail comparable to those from the HST at Koper 4.

In their study on size changes of *V. gibba,* Tomašových et al. (2020) included material from a much longer (26 m) core from the Po plain area reaching Lower to Middle Holocene marine sediments currently buried under the prograding Po delta. The record from this core is comparable to Po 3, Po 4, and Panzano in its degree of time averaging. Size distributions of *V. gibba* differed between death assemblages from the pre-20th-century Holocene of the Po plain and those from the late 20th century of Po 3, Po 4, and Panzano. This indicates that there was truly a regime shift in size structure of *V. gibba*.

Size distributions of *T. tricarinata* from high-resolution records extending back to the earlier Holocene would be equally valuable to study long-term trends in this species. However, even the century- to millennial-scale time averaged Holocene record at Koper 4 has a variability in size distributions that strongly overlaps with that from the late 20th century in the NAS. Therefore, it can be concluded that there was no basin-wide regime shift in the size structure of *T. tricarinata* during the late 20th century. The comparison of size trends of *V. gibba* and *T. tricarinata* demonstrates how differently this important functional trait is affected by anthropogenic stressors depending on the ecological characteristics of a species.

Conclusions

This study examined the size changes of two mollusk species, the bivalve *Varicorbula gibba* and the gastropod *Turritellinella tricarinata*, in response to natural environmental shifts and anthropogenic impacts during the Holocene, based on sediment cores from four stations within the northern Adriatic Sea (NAS).

Long-term trends were analyzed using newly described material from station Koper 4 in the southern Gulf of Trieste, extending the record back more than 7,000 years to the late transgressive phase. Community composition changed as the sediment got coarser at the transition from the transgressive phase and the time of maximum flooding to the highstand phase. *V. gibba* and *T. tricarinata* remained abundant throughout these phases but changed in size. *V. gibba* increased in size

during the highstand phase, possibly benefiting from the onset of modern circulation patterns in the NAS, which could have increased the frequency of hypoxic events. These events likely led to populations with a high frequency of large individuals, thereby increasing the average size of the time-averaged death assemblages found at Koper 4.

In contrast, *T. tricarinata* exhibited smaller sizes for most of the highstand phase compared to the earlier Holocene. Potential drivers of this size decrease include an increase in drilling predation and a decrease in nutrient input. While some size distributions from the early highstand phase are dominated by large individuals, these assemblages may have resulted from size sorting by high-energy events rather than recording an ecological signal.

Records from the other three stations, located in the Isonzo and Po prodeltas, corroborate previous findings that *V. gibba* increased in size in response to eutrophication and a higher frequency of hypoxia during the late 20th century. The prevalence of large individuals suggests higher survival rates during this period, indicating a release from predation or competition. The larger sizes observed at stations in the eutrophic Po prodelta also suggest that increased nutrient input may have contributed to this size increase.

In contrast, *T. tricarinata* did not exhibit a uniform size response to the stressors of the 20th century. Unlike *V. gibba*, *T. tricarinata* declined in abundance, potentially leading to local extirpations in some areas, while in others, lower abundances resulted in recruitment failure and populations dominated by large-sized adults. While the late 20th-century size structure of *V. gibba* is unique within the Holocene of the NAS, recent size changes in *T. tricarinata* fall within the natural range of variability of this species during the Holocene. Thus, size responses to anthropogenic stressors vary strongly between species with different ecological characteristics.

Acknowledgements

I would like to express my gratitude to Ivana Koubová from the Earth Science Institute of the Slovak Academy of Sciences in Bratislava for her meticulous measurements of specimens from stations Po 4, Panzano, and Koper 4, which provided new data for this study. My thanks also go to Adam Tomašových from the same institute for sharing valuable insights on previously published data and offering crucial advice on methods and analyses. I am equally grateful to Paolo Albano from the Anton Dohrn Zoological Station in Naples for providing information on previously published data. I wish to thank Roberto Zonta, Daniele Cassin, and Simone Leoni from the Institute of Marine Research in Venice for their contribution of geochemical data from station Koper 4. From our working group at the Conservation Paleobiology and Historical Ecology Lab at the University of Vienna, I thank Bettina Bachmann for sieving the material from Koper 4 and providing grain size data, and Matej Pavlović for assisting with species identification for

station Koper 4. Finally, I would like to extend my deepest appreciation to my supervisors Rafał Nawrot and Martin Zuschin for their guidance, patience, and support throughout this project, as well as for facilitating the presentation of my findings at various conferences.

References

Albano, P.G., Gallmetzer, I., Haselmair, A., Tomašových, A., Stachowitsch, M., Zuschin, M., 2018. Historical ecology of a biological invasion: the interplay of eutrophication and pollution determines time lags in establishment and detection. Biol. Invasions 20, 1417–1430. https://doi.org/10.1007/s10530-017-1634-7

Allmon, W.D., 2011. Natural History of Turritelline Gastropods (Cerithiodea: Turritellidae): A Status Report. Malacologia 54, 159–202. https://doi.org/10.4002/040.054.0107

Allmon, W.D., 1988. Ecology of Recent Turritelline Gastropods (Prosobranchia, Turritellidae): Current Knowledge and Paleontological Implications. PALAIOS 3, 259. https://doi.org/10.2307/3514657

Altieri, A.H., Diaz, R.J., 2019. Dead Zones: Oxygen Depletion in Coastal Ecosystems, in: World Seas: An Environmental Evaluation. Elsevier, pp. 453–473. https://doi.org/10.1016/B978-0-12-805052-1.00021-8

Altieri, A.H., Witman, J.D., 2006. Local Extinction of a Foundation Species in a Hypoxic Estuary: Integrating Individuals to Ecosystem. Ecology 87, 717–730. https://doi.org/10.1890/05-0226

Amorosi, A., Bruno, L., Campo, B., Morelli, A., Rossi, V., Scarponi, D., Hong, W., Bohacs, K.M., Drexler, T.M., 2017. Global sea-level control on local parasequence architecture from the Holocene record of the Po Plain, Italy. Mar. Pet. Geol., Sedimentology in Italy: recent advances and insights 87, 99–111. https://doi.org/10.1016/j.marpetgeo.2017.01.020

Asioli, A., Trincardi, F., Correggiari, A., Langone, L., Vigliotti, L., Van Der Kaars, S., Lowe, J., 1996. The late Quaternary deglaciation in the Central Adriatic basin. Alp. Mediterr. Quat. 9, 763–769.

Basset, A., Sabetta, L., Sangiorgio, F., Pinna, M., Migoni, D., Fanizzi, F., Barbone, E., Galuppo, N., Fonda Umani, S., Reizopoulou, S., Nicolaidou, A., Arvanitidis, C., Moncheva, S., Trajanova, A., Georgescu, L., Beqiraj, S., 2008. Biodiversity conservation in Mediterranean and Black Sea lagoons: a trait-oriented approach to benthic invertebrate guilds. Aquat. Conserv. Mar. Freshw. Ecosyst. 18, S4–S15. https://doi.org/10.1002/aqc.979

Bright, J., Ebert, C., Flores, C., Harnik, P.G., Huntley, J.W., Kowalewski, M., Portell, R.W., Retelle, M., Schuur, E.A.G., Kaufman, D.S., 2024. Comparing MICADAS Gas Source, Direct Carbonate, and Standard Graphite ^{14} C Determinations of Biogenic Carbonate. Radiocarbon 66, 295–305. https://doi.org/10.1017/RDC.2024.45

Buchman, M.F., 2008. Screening Quick Reference Table (SQuiRTs). NOAA R Rep. 08–1.

Burton, Jr., G. Allen, 2002. Sediment quality criteria in use around the world. Limnology 3,

65–76. https://doi.org/10.1007/s102010200008

Calderaro, L.A., Harnik, P.G., Rillo, M.C., 2023. Environmental correlates of molluscan predator–prey body size in the northern Gulf of Mexico. Paleobiology 1–15. https://doi.org/10.1017/pab.2023.22

Carmichael, R.H., Shriver, A.C., Valiela, I., 2012. Bivalve Response to Estuarine Eutrophication: The Balance between Enhanced Food Supply and Habitat Alterations. J. Shellfish Res. 31, 1–11. https://doi.org/10.2983/035.031.0101

Chiantore, M., Bedulli, D., Cattaneo-Vietti, R., Schiaparelli, S., Albertelli, G., 2001. Long-term changes in the Mollusc-Echinoderm assemblages in the north and coastal middle Adriatic Sea. Atti Della Assoc. Ital. Oceanol. E Limnol. 14, 63–75.

Clark, M.S., Husmann, G., Thorne, M.A.S., Burns, G., Truebano, M., Peck, L.S., Abele, D., Philipp, E.E.R., 2013. Hypoxia impacts large adults first: consequences in a warming world. Glob. Change Biol. 19, 2251–2263. https://doi.org/10.1111/gcb.12197

Craig, N., 1994. Growth of the bivalve Nucula annulata in nutrient-enriched environments. Mar. Ecol. Prog. Ser. 104, 77–90. https://doi.org/10.3354/meps104077

Crema, E.R., Bevan, A., 2021. Inference from large sets of radiocarbon dates: software and methods. Radiocarbon 63, 23–39.

Crema, R., Castelli, A., Prevedelli, D., 1991. Long term eutrophication effects on macrofaunal communities in northern Adriatic Sea. Mar. Pollut. Bull. 22, 503–508. https://doi.org/10.1016/0025-326X(91)90405-H

De Baets, K., Jarochowska, E., Buchwald, S.Z., Klug, C., Korn, D., 2022. Lithology controls ammonoid size distribution. PALAIOS 37, 744–754. https://doi.org/10.2110/palo.2021.063

Dietl, G.P., Kidwell, S.M., Brenner, M., Burney, D.A., Flessa, K.W., Jackson, S.T., Koch, P.L., 2015. Conservation Paleobiology: Leveraging Knowledge of the Past to Inform Conservation and Restoration. Annu. Rev. Earth Planet. Sci. 43, 79–103. https://doi.org/10.1146/annurev-earth-040610-133349

Frignani, M., Langone, L., Ravaioli, M., Sorgente, D., Alvisi, F., Albertazzi, S., 2005. Fine-sediment mass balance in the western Adriatic continental shelf over a century time scale. Mar. Geol. 222–223, 113–133. https://doi.org/10.1016/j.margeo.2005.06.016

Fuksi, T., Tomašových, A., Gallmetzer, I., Haselmair, A., Zuschin, M., 2018. 20th century increase in body size of a hypoxia-tolerant bivalve documented by sediment cores from the northern Adriatic Sea (Gulf of Trieste). Mar. Pollut. Bull. 135, 361–375. https://doi.org/10.1016/j.marpolbul.2018.07.004

Gallmetzer, I., Haselmair, A., Stachowitsch, M., Zuschin, M., 2016. An innovative piston corer for large-volume sediment samples. Limnol. Oceanogr. Methods 14, 698–717. https://doi.org/10.1002/lom3.10124

Gallmetzer, I., Haselmair, A., Tomašových, A., Mautner, A.-K., Schnedl, S.-M., Cassin, D., Zonta, R., Zuschin, M., 2019. Tracing origin and collapse of Holocene benthic baseline communities in the northern Adriatic Sea. PALAIOS 34, 121–145. https://doi.org/10.2110/palo.2018.068

Gallmetzer, I., Haselmair, A., Tomašových, A., Stachowitsch, M., Zuschin, M., 2017. Responses of molluscan communities to centuries of human impact in the northern Adriatic Sea. PLOS ONE 12, e0180820. https://doi.org/10.1371/journal.pone.0180820

Giani, M., Djakovac, T., Degobbis, D., Cozzi, S., Solidoro, C., Umani, S.F., 2012. Recent changes in the marine ecosystems of the northern Adriatic Sea. Estuar. Coast. Shelf Sci. 115, 1–13. https://doi.org/10.1016/j.ecss.2012.08.023

Hagadorn, J.W., Boyajian, G.E., 1997. Subtle Changes in Mature Predator-Prey Systems: An Example from Neogene Turritella (Gastropoda). PALAIOS 12, 372. https://doi.org/10.2307/3515336

Haselmair, A., Gallmetzer, I., Tomašových, A., Wieser, A., Übelhör, A., Zuschin, M., 2021. Basin-wide infaunalisation of benthic soft-bottom communities driven by anthropogenic habitat degradation in the northern Adriatic Sea. Mar. Ecol. Prog. Ser. 671, 45–65. https://doi.org/10.3354/meps13759

Heaton, T.J., Köhler, P., Butzin, M., Bard, E., Reimer, R.W., Austin, W.E.N., Bronk Ramsey, C., Grootes, P.M., Hughen, K.A., Kromer, B., Reimer, P.J., Adkins, J., Burke, A., Cook, M.S., Olsen, J., Skinner, L.C., 2020. Marine20—The Marine Radiocarbon Age Calibration Curve (0–55,000 cal BP). Radiocarbon 62, 779–820. https://doi.org/10.1017/RDC.2020.68

Holmes, S., Miller, N., 2006. Aspects of the ecology and population genetics of the bivalve Corbula gibba. Mar. Ecol. Prog. Ser. 315, 129–140. https://doi.org/10.3354/meps315129

Hrs-Brenko, M., 2006. The basket shell, Corbula gibba Olivi, 1792 (Bivalve Mollusks) as a species resistant to environmental disturbances: A review. ACTA Adriat. 47, 49–64.

Jackson, J.B.C., 2001. What was natural in the coastal oceans? Proc. Natl. Acad. Sci. 98, 5411–5418. https://doi.org/10.1073/pnas.091092898

Johannessen, S.C., Macdonald, R.W., 2012. There is no 1954 in that core! Interpreting sedimentation rates and contaminant trends in marine sediment cores. Mar. Pollut. Bull. 64, 675–678. https://doi.org/10.1016/j.marpolbul.2012.01.026

Justić, D., 1991. Hypoxic conditions in the northern Adriatic Sea: historical development and ecological significance. Geol. Soc. Lond. Spec. Publ. 58, 95–105. https://doi.org/10.1144/GSL.SP.1991.058.01.07

Kardon, G., 1998. Evidence from the Fossil Record of an Antipredatory Exaptation: Conchiolin Layers in Corbulid Bivalves. Evolution 52, 68–79. https://doi.org/10.2307/2410921

Kidwell, S.M., 2015. Biology in the Anthropocene: Challenges and insights from young fossil records. Proc. Natl. Acad. Sci. 112, 4922–4929. https://doi.org/10.1073/pnas.1403660112

Kidwell, S.M., 2013. Time-averaging and fidelity of modern death assemblages: building a taphonomic foundation for conservation palaeobiology. Palaeontology 56, 487–522. https://doi.org/10.1111/pala.12042

Kidwell, S.M., 2009. Evaluating human modifications of shallow marine ecosystems: mismatch in composition of molluscan living and time-averaged death assemblages.

Conserv. Paleobiology Using Past Manage Future Paleontol. Soc. Short Course Oct. 17th 2009 Paleontol. Soc. Pap. 15.

Kidwell, S.M., Tomasovych, A., 2013. Implications of Time-Averaged Death Assemblages for Ecology and Conservation Biology. Annu. Rev. Ecol. Evol. Syst. 44, 539–563. https://doi.org/10.1146/annurev-ecolsys-110512-135838

Kosnik, M.A., Kowalewski, M., 2016. Understanding modern extinctions in marine ecosystems: the role of palaeoecological data. Biol. Lett. 12, 20150951. https://doi.org/10.1098/rsbl.2015.0951

Kowalewski, M., Wittmer, J.M., Dexter, T.A., Amorosi, A., Scarponi, D., 2015. Differential responses of marine communities to natural and anthropogenic changes. Proc. R. Soc. B Biol. Sci. 282, 20142990. https://doi.org/10.1098/rspb.2014.2990

Kralj, M., Lipizer, M., Čermelj, B., Celio, M., Fabbro, C., Brunetti, F., Francé, J., Mozetič, P., Giani, M., 2019. Hypoxia and dissolved oxygen trends in the northeastern Adriatic Sea (Gulf of Trieste). Deep Sea Res. Part II Top. Stud. Oceanogr. 164, 74–88. https://doi.org/10.1016/j.dsr2.2019.06.002

Krause, R.A., Barbour, S.L., Kowalewski, M., Kaufman, D.S., Romanek, C.S., Simões, M.G., Wehmiller, J.F., 2010. Quantitative comparisons and models of time-averaging in bivalve and brachiopod shell accumulations. Paleobiology 36, 428–452. https://doi.org/10.1666/08072.1

Lotze, H.K., Coll, M., Dunne, J.A., 2011. Historical Changes in Marine Resources, Food-web Structure and Ecosystem Functioning in the Adriatic Sea, Mediterranean. Ecosystems 14, 198–222. https://doi.org/10.1007/s10021-010-9404-8

Marsden, I.D., Shumway, S.E., Padilla, D.K., 2012. Does size matter? The effects of body size and declining oxygen tension on oxygen uptake in gastropods. J. Mar. Biol. Assoc. U. K. 92, 1603–1617. https://doi.org/10.1017/S0025315411001512

Mautner, A.-K., Gallmetzer, I., Haselmair, A., Schnedl, S.-M., Tomašových, A., Zuschin, M., 2018. Holocene ecosystem shifts and human-induced loss of Arca and Ostrea shell beds in the north-eastern Adriatic Sea. Mar. Pollut. Bull. 126, 19–30. https://doi.org/10.1016/j.marpolbul.2017.10.084

McKinney, F.K., 2007. The northern Adriatic ecosystem: deep time in a shallow sea. Columbia University Press.

Menard, H.W., Boucot, A.J., 1951. Experiments on the movement of shells by water. Am. J. Sci. 249, 131–151.

Moraitis, M.L., Tsikopoulou, I., Geropoulos, A., Dimitriou, P.D., Papageorgiou, N., Giannoulaki, M., Valavanis, V.D., Karakassis, I., 2018. Molluscan indicator species and their potential use in ecological status assessment using species distribution modeling. Mar. Environ. Res. 140, 10–17. https://doi.org/10.1016/j.marenvres.2018.05.020

Nawrot, R., Berensmeier, M., Gallmetzer, I., Haselmair, A., Tomašových, A., Zuschin, M., 2022. Multiple phyla, one time resolution? Similar time averaging in benthic foraminifera, mollusk, echinoid, crustacean, and otolith fossil assemblages. Geology 50, 902–906. https://doi.org/10.1130/G49970.1

Nerlović, V., Doğan, A., Hrs-Brenko, M., 2011. Response to oxygen deficiency (depletion): Bivalve assemblages as an indicator of ecosystem instability in the northern Adriatic Sea. Biologia (Bratisl.) 66, 1114–1126. https://doi.org/10.2478/s11756-011-0121-3

Ogorelec, B., Mišič, M., Faganeli, J., 1991. Marine geology of the Gulf of Trieste (northern Adriatic): Sedimentological aspects. Mar. Geol. 99, 79–92.

Oksanen, J., Simpson, G.L., Blanchet, F.G., Kindt, R., Legendre, P., Minchin, P.R., O'Hara, R.B., Solymos, P., Stevens, M.H.H., Szoecs, E., Wagner, H., Barbour, M., Bedward, M., Bolker, B., Borcard, D., Carvalho, G., Chirico, M., Caceres, M.D., Durand, S., Evangelista, H.B.A., FitzJohn, R., Friendly, M., Furneaux, B., Hannigan, G., Hill, M.O., Lahti, L., McGlinn, D., Ouellette, M.-H., Cunha, E.R., Smith, T., Stier, A., Braak, C.J.F.T., Weedon, J., 2024. vegan: Community Ecology Package.

Peharda, M., Sironić, A., Markulin, K., Jozić, S., Borković, D., Andersson, C., 2019. The Bivalve *Glycymeris pilosa* as an Archive of ^{14} C in the Mediterranean Sea. Radiocarbon 61, 599–613. https://doi.org/10.1017/RDC.2018.146

Piva, A., Asioli, A., Trincardi, F., Schneider, R.R., Vigliotti, L., 2008. Late-Holocene climate variability in the Adriatic sea (Central Mediterranean). The Holocene 18, 153–167.

Queirós, A.M., Hiddink, J.G., Kaiser, M.J., Hinz, H., 2006. Effects of chronic bottom trawling disturbance on benthic biomass, production and size spectra in different habitats. J. Exp. Mar. Biol. Ecol. 335, 91–103. https://doi.org/10.1016/j.jembe.2006.03.001

R Core Team, 2024. R: A Language and Environment for Statistical Computing. R Foundation for Statistical Computing, Vienna.

Rice, J., Arvanitidis, C., Borja, A., Frid, C., Hiddink, J.G., Krause, J., Lorance, P., Ragnarsson, S.Á., Sköld, M., Trabucco, B., Enserink, L., Norkko, A., 2012. Indicators for Sea-floor Integrity under the European Marine Strategy Framework Directive. Ecol. Indic. 12, 174–184. https://doi.org/10.1016/j.ecolind.2011.03.021

Rick, T.C., Erlandson, J.M., 2008. Human Impacts on Ancient Marine Ecosystems : A Global Perspective. University of California Press, Berkeley.

Riedel, B., Zuschin, M., Stachowitsch, M., 2012. Tolerance of benthic macrofauna to hypoxia and anoxia in shallow coastal seas: a realistic scenario. Mar. Ecol. Prog. Ser. 458, 39–52. https://doi.org/10.3354/meps09724

Ruckdeschel, P., Kohl, M., Stabla, T., Camphausen, F., 2006. S4 classes for distributions. R News 6, 2–6.

Sanchez-Cabeza, J.A., Ruiz-Fernández, A.C., 2012. 210Pb sediment radiochronology: An integrated formulation and classification of dating models. Geochim. Cosmochim. Acta, Environmental Records of Anthropogenic Impacts 82, 183–200. https://doi.org/10.1016/j.gca.2010.12.024

Scheidl, A., Berensmeier, M., Nawrot, R., Albano, P.G., Tomašových, A., Zuschin, M., 2021. Stratigraphic changes in shell size of a turritellid gastropod in the Holocene fossil record of the Po prodelta (Northern Adriatic Sea). EGU General Assembly 2021, online, 19–30 Apr 2021, EGU21-9604. https://doi.org/10.5194/egusphere-egu21-9604.

Shin, C.P., Allmon, W.D., Anderson, B.M., Kelly, B.T., Hiscock, K., Shin, P.K.S., 2020.

Distribution and abundance of turritelline gastropods (Cerithioidea: Turritellidae) in Hong Kong and the English Channel: implications for a characteristic fossil assemblage. J. Mar. Biol. Assoc. U. K. 100, 1261–1270. https://doi.org/10.1017/S0025315420001204

Siani, G., Paterne, M., Arnold, M., Bard, E., Métivier, B., Tisnerat, N., Bassinot, F., 2000. Radiocarbon Reservoir Ages in the Mediterranean Sea and Black Sea. Radiocarbon 42, 271–280. https://doi.org/10.1017/S0033822200059075

Synal, H.-A., Stocker, M., Suter, M., 2007. MICADAS: A new compact radiocarbon AMS system. Nucl. Instrum. Methods Phys. Res. Sect. B Beam Interact. Mater. At. 259, 7–13. https://doi.org/10.1016/j.nimb.2007.01.138

Tomašových, A., Albano, P.G., Fuksi, T., Gallmetzer, I., Haselmair, A., Kowalewski, M., Nawrot, R., Nerlović, V., Scarponi, D., Zuschin, M., 2020. Ecological regime shift preserved in the Anthropocene stratigraphic record. Proc. R. Soc. B Biol. Sci. 287, 20200695. https://doi.org/10.1098/rspb.2020.0695

Tomašových, A., Gallmetzer, I., Haselmair, A., Kaufman, D.S., Kralj, M., Cassin, D., Zonta, R., Zuschin, M., 2018. Tracing the effects of eutrophication on molluscan communities in sediment cores: outbreaks of an opportunistic species coincide with reduced bioturbation and high frequency of hypoxia in the Adriatic Sea. Paleobiology 44, 575–602. https://doi.org/10.1017/pab.2018.22

Tomašových, A., Gallmetzer, I., Haselmair, A., Kaufman, D.S., Mavrič, B., Zuschin, M., 2019. A decline in molluscan carbonate production driven by the loss of vegetated habitats encoded in the Holocene sedimentary record of the Gulf of Trieste. Sedimentology 66, 781–807. https://doi.org/10.1111/sed.12516

Tomašových, A., Gallmetzer, I., Haselmair, A., Kaufman, D.S., Vidović, J., Zuschin, M., 2017. Stratigraphic unmixing reveals repeated hypoxia events over the past 500 yr in the northern Adriatic Sea. Geology 45, 363–366. https://doi.org/10.1130/G38676.1

Trobec, A., Busetti, M., Zgur, F., Baradello, L., Babich, A., Cova, A., Gordini, E., Romeo, R., Tomini, I., Poglajen, S., Diviacco, P., Vrabec, M., 2018. Thickness of marine Holocene sediment in the Gulf of Trieste (northern Adriatic Sea). Earth Syst. Sci. Data 10, 1077–1092. https://doi.org/10.5194/essd-10-1077-2018

Tull, D.S., Böhning-Gaese, K., 1993. Patterns of drilling predation on gastropods of the family Turritellidae in the Gulf of California. Paleobiology 19, 476–486. https://doi.org/10.1017/S0094837300014093

Tunnicliffe, V., 1981. High species diversity and abundance of the epibenthic community in an oxygen-deficient basin. Nature 294, 354–356. https://doi.org/10.1038/294354a0

Tyler, C.L., Kowalewski, M., 2017. Surrogate taxa and fossils as reliable proxies of spatial biodiversity patterns in marine benthic communities. Proc. R. Soc. B Biol. Sci. 284, 20162839. https://doi.org/10.1098/rspb.2016.2839

Vacchi, M., Marriner, N., Morhange, C., Spada, G., Fontana, A., Rovere, A., 2016. Multiproxy assessment of Holocene relative sea-level changes in the western Mediterranean: Sea-level variability and improvements in the definition of the isostatic signal. Earth-Sci. Rev. 155, 172–197. https://doi.org/10.1016/j.earscirev.2016.02.002

Venables, W.N., Ripley, B.D., 2002. Modern Applied Statistics with S, Springer, New York: ISBN 0-387-95457-0.

Vidović, J., Nawrot, R., Gallmetzer, I., Haselmair, A., Tomašových, A., Stachowitsch, M., Ćosović, V., Zuschin, M., 2016. Anthropogenically induced environmental changes in the northeastern Adriatic Sea in the last 500 years (Panzano Bay, Gulf of Trieste). Biogeosciences 13, 5965–5981. https://doi.org/10.5194/bg-13-5965-2016

Yonge, C.M., 1946. On the Habits and Adaptations of *Aloidis (Corbula) Gibba*. J. Mar. Biol. Assoc. U. K. 26, 358–376. https://doi.org/10.1017/S0025315400012182

Zavatarelli, M., Raicich, F., Bregant, D., Russo, A., Artegiani, A., 1998. Climatological biogeochemical characteristics of the Adriatic Sea. J. Mar. Syst. 18, 227–263. https://doi.org/10.1016/S0924-7963(98)00014-1

Zuschin, M., Harzhauser, M., Mandic, O., 2005. Influence of Size-sorting on Diversity Estimates from Tempestitic Shell Beds in the Middle Miocene of Austria. PALAIOS 20, 142–158. https://doi.org/10.2110/palo.2003.p03-87

Zuschin, M., Nawrot, R., Dengg, M., Gallmetzer, I., Haselmair, A., Kowalewski, M., Scarponi, D., Wurzer, S., Tomašových, A., in press. Human-driven breakdown of predator-prey interactions in the northern Adriatic Sea. Proc. R. Soc. B Biol. Sci.

Zuschin, M., Nawrot, R., Dengg, M., Gallmetzer, I., Haselmair, A., Wurzer, S., Tomašových, A., 2022. Scale dependence of drilling predation in the Holocene of the northern Adriatic Sea across benthic habitats and nutrient regimes. Paleobiology 48, 462–479. https://doi.org/10.1017/pab.2022.6

Appendix

Sample sizes of measured V. gibba *specimens for original increments (as they were sliced on board after collection). Note small sample sizes of some increments from the upper part of cores from station Po 3 and Po 4.*

	Po 3	Po 4	Panzano		Koper 4
0-2 cm	1	14	54	**0-2.5 cm**	89
2-4 cm	4	5	58	**2.5-5 cm**	113
4-6 cm	6	12	79	**5-7.5 cm**	133
6-8 cm	9	22	76	**7.5-10 cm**	120
8-10 cm	11	7	66	**10-12.5 cm**	201
10-12 cm	19	3	83	**12.5-15 cm**	113
12-14 cm	16	9	96	**15-17.5 cm**	190
14-16 cm	18	10	90	**17.5-20 cm**	217
16-18 cm	17	13	57	**20-25 cm**	200
18-20 cm	17	3	36	**25-30 cm**	258
20-25 cm	45	43	80	**30-35 cm**	162
25-30 cm	20	61	114	**35-40 cm**	154
30-35 cm	29	48	100	**40-45 cm**	159
35-40 cm	15	34	123	**45-50 cm**	80
40-45 cm	42	44	195	**50-55 cm**	300
45-50 cm	28	61	92	**55-60 cm**	141
50-55 cm	32	31	56	**60-65 cm**	74
55-60 cm	33	34	46	**65-70 cm**	55
60-65 cm	25	70	64	**70-75 cm**	97
65-70 cm	40	28	25	**75-80 cm**	74
70-75 cm	40	43	35	**80-85 cm**	141
75-80 cm	24	70	49	**85-90 cm**	115
80-85 cm	39	26	11	**90-95 cm**	205
85-90 cm	21	8	31	**95-100 cm**	227
90-95 cm	10	38	40	**100-105 cm**	151
95-100 cm	46	7	45	**105-110 cm**	192
100-105 cm	13	14	87	**110-115 cm**	123
105-110 cm	16	26	62	**115-120 cm**	218
110-115 cm	19	8	62	**120-125 cm**	214
115-120 cm	5	9	69	**125-130 cm**	158
120-125 cm	3	6	71	**130-135 cm**	193
125-130 cm	1	11	69	**135-140 cm**	209
130-135 cm	14	12	102	**140-145 cm**	150
135-140 cm	14	3	68	**145-150 cm**	120
140-145 cm	3	2	34		
145-150 cm	2	2	40		
150-155 cm	1	6			

Sample sizes of measured T. tricarinata *specimens for original increments (as they were sliced on board after collection). Note small sample sizes of some increments from the upper part of cores from station Po 3, Po 4, and Panzano.*

	Po 3	Po 4	Panzano		Koper 4
0-2 cm	0	1	2	**0-2.5 cm**	14
2-4 cm	0	0	3	**2.5-5 cm**	13
4-6 cm	0	1	4	**5-7.5 cm**	19
6-8 cm	0	4	2	**7.5-10 cm**	16
8-10 cm	0	0	3	**10-12.5 cm**	39
10-12 cm	0	2	2	**12.5-15 cm**	12
12-14 cm	0	0	12	**15-17.5 cm**	9
14-16 cm	0	1	11	**17.5-20 cm**	22
16-18 cm	0	2	20	**20-25 cm**	20
18-20 cm	0	0	17	**25-30 cm**	17
20-25 cm	2	4	23	**30-35 cm**	17
25-30 cm	2	3	43	**35-40 cm**	16
30-35 cm	3	2	31	**40-45 cm**	11
35-40 cm	0	6	42	**45-50 cm**	8
40-45 cm	1	6	47	**50-55 cm**	50
45-50 cm	10	3	29	**55-60 cm**	31
50-55 cm	1	2	24	**60-65 cm**	26
55-60 cm	3	4	19	**65-70 cm**	16
60-65 cm	4	7	17	**70-75 cm**	38
65-70 cm	7	5	10	**75-80 cm**	16
70-75 cm	3	6	5	**80-85 cm**	40
75-80 cm	5	3	10	**85-90 cm**	30
80-85 cm	1	6	7	**90-95 cm**	40
85-90 cm	17	7	19	**95-100 cm**	38
90-95 cm	8	17	30	**100-105 cm**	35
95-100 cm	16	11	26	**105-110 cm**	44
100-105 cm	7	9	40	**110-115 cm**	43
105-110 cm	8	5	28	**115-120 cm**	42
110-115 cm	9	7	39	**120-125 cm**	47
115-120 cm	7	13	58	**125-130 cm**	26
120-125 cm	9	6	22	**130-135 cm**	34
125-130 cm	10	10	20	**135-140 cm**	34
130-135 cm	12	8	41	**140-145 cm**	14
135-140 cm	8	5	43	**145-150 cm**	17
140-145 cm	8	7	26		
145-150 cm	7	3	21		
150-155 cm	2	0			

The median and 95th percentile size (in mm) of V. gibba *and* T. tricarinata *from major temporal/stratigraphic units of all studied stations.*

		V. gibba		***T. tricarinata***	
Station	**Unit**	**Median**	**95th percentile**	**Median**	**95th percentile**
Po 3	Early 21st century	4.51	9.69	NA	NA
	Late 20th century	8.29	11.99	14.32	33.38
	Early 20th century	3.36	8.70	6.19	37.08
Po 4	Early 21st century	4.97	11.24	16.13	21.95
	Late 20th century	5.77	11.78	23.77	37.88
	Early 20th century	3.11	6.16	5.05	39.32
Panzano	20th to 21st century	4.03	11.34	5.35	44.81
	19th century	3.22	8.70	4.92	36.64
	18th century	3.00	7.80	4.63	34.15
	17th century	3.19	8.74	5.21	39.29
Koper 4	HST	3.20	9.60	5.28	42.22
	TST-MFZ	3.25	7.56	6.07	31.50

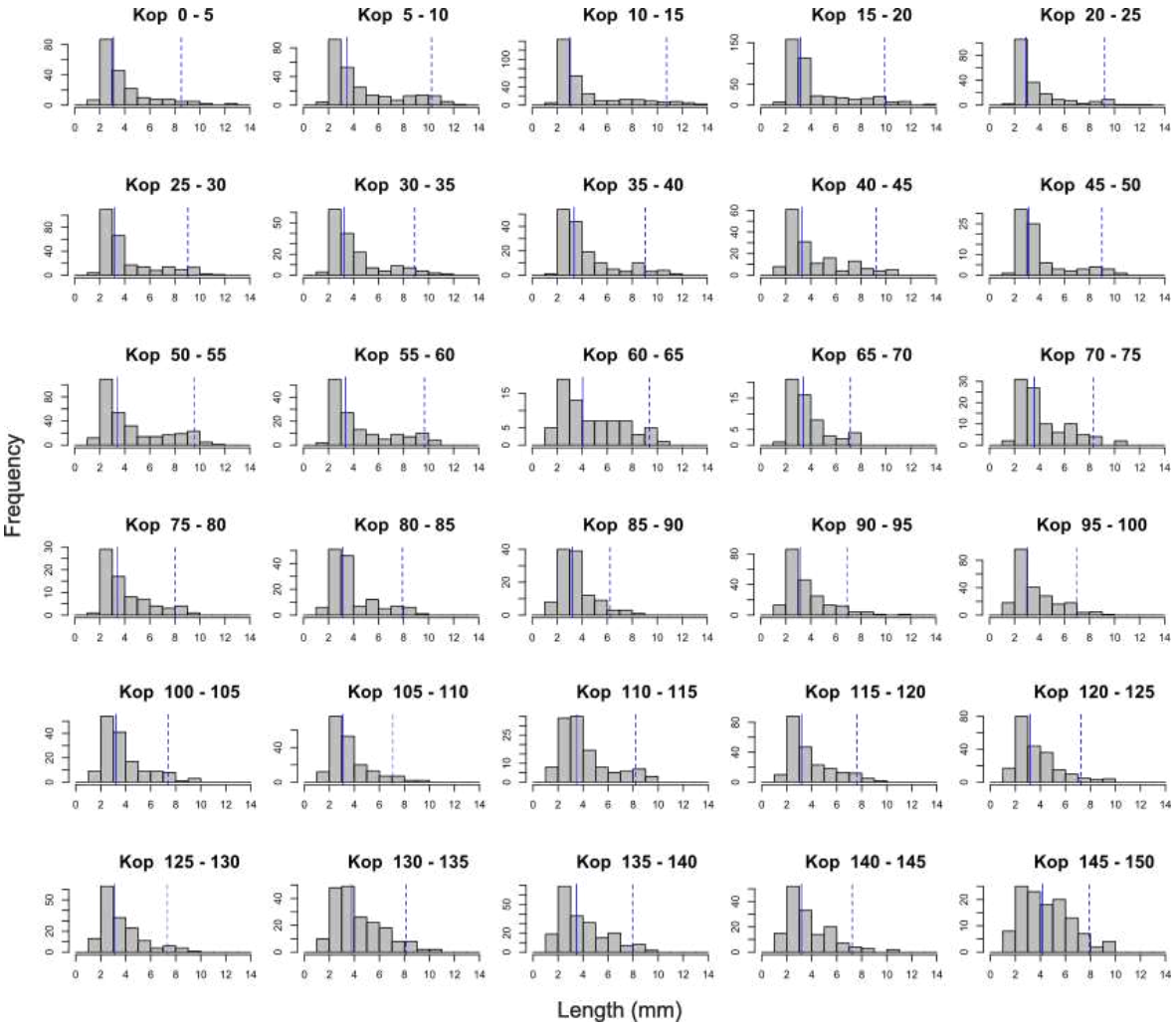

Size distributions of V. gibba *from 5-cm-increments from station Koper 4. These increments were used for NMDS of size distributions of* V. gibba *based on Kolmogorov distances (figure 25), together with the size distributions from the temporal units of stations Po 3, Po 4, and Panzano (figures 17, 19, 21). The solid line indicates the median, the dashed line the 95th percentile length. Note the difference in scale of frequency of the histograms.*

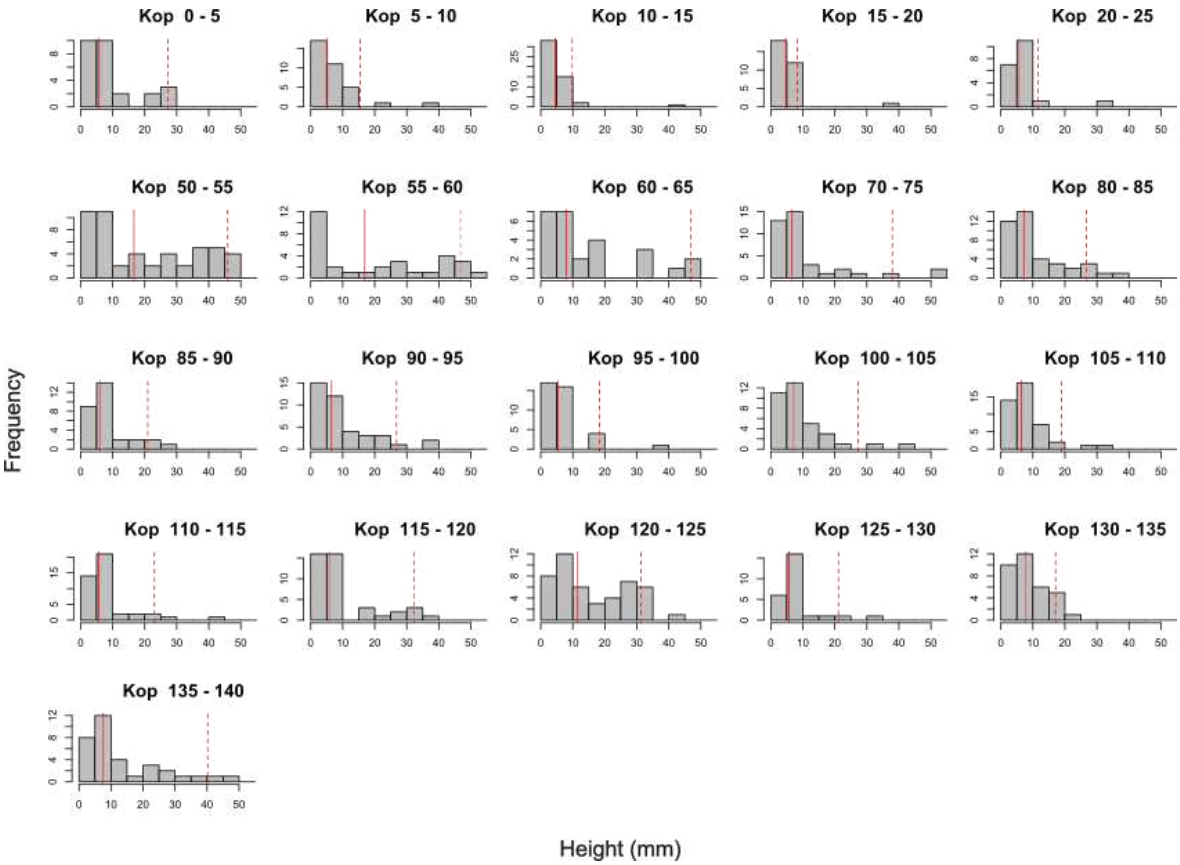

Size distributions of T. tricarinata *from 5-cm-increments from station Koper 4. These increments were used for NMDS of size distributions of* T. tricarinata *based on Kolmogorov distances (figure 26), together with the size distributions form the temporal units of stations Po 3, Po 4, and Panzano (figures 17, 19, 21). Some 5-cm-increments were omitted from the analysis because their sample size was below 20. The solid line indicates the median, the dashed line the 95th percentile height. Note the difference in scale of frequency of the histograms.*